

# **DIGITAL DISTANCE PROTECTION SCHEME FOR SERIES COMPENSATED TRANSMISSION LINES**

**A DISSERTATION**

*Submitted in partial fulfillment of the  
requirements for the award of the degree*

*of*

**MASTER OF TECHNOLOGY**

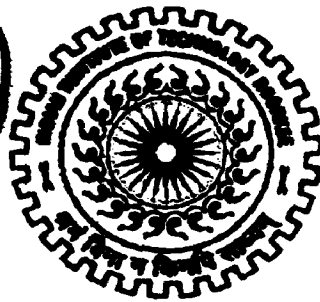
*in*

**ELECTRICAL ENGINEERING**

**(With Specialization in Power System Engineering)**

**By**

**PARIKH URMIL BHAGAVANDAS**



**DEPARTMENT OF ELECTRICAL ENGINEERING  
INDIAN INSTITUTE OF TECHNOLOGY ROORKEE**

**ROORKEE -247 667 (INDIA)**

**MAY, 2007**

## **CANDIDATE'S DECLARATION**

---

I hereby declare that the work presented in this dissertation titled "**Digital Distance Protection Scheme for Series Compensated Transmission Lines**" submitted in partial fulfilment of the requirement for the award of the **Master of technology**, in **Electrical Engineering**, with specialization in **Power System Engineering**, in the **Department of Electrical Engineering, Indian Institute of Technology, Roorkee**, is an authentic record of my own work, carried out effect from June 2006 to May 2007 under the guidance of **Dr. Biswarup Das and Dr. R. P. Maheshwari, Department of Electrical Engineering, IIT Roorkee**.

The matter embodied in this thesis has not been submitted for the award of any other degree.

Date: <sup>st</sup>21, May, 2007.

Place: Roorkee



(PARIKH URMIL B.)

---

## **CERTIFICATE**

This is to certify that the above statement made by the candidate is correct to best of our knowledge and belief.



---

**(Dr. R. P. Maheshwari)**  
Associate Professor  
Dept. of Electrical Engineering  
Indian Institute of Technology,  
Roorkee – 247 667, India.



---

**(Dr. Biswarup Das)**  
Associate Professor  
Dept. of Electrical Engineering  
Indian Institute of Technology,  
Roorkee – 247 667, India.

## **ACKNOWLEDGEMENTS**

---

I dedicate this dissertation report to my wife Purvi, my little daughter Kashvi and my parents without whom I have no origin.

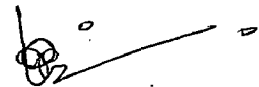
I take this opportunity to express my profound gratitude to Professor Dr. Biswarup Das and Prof. Dr. R. P. Maheshwari, Department of Electrical Engineering, IIT Roorkee, under whose guidance this dissertation work was carried out. Without their support, encouragement and vigilant guidance completion of this dissertation would have been impossible.

I would like to acknowledge Prof. Dr. S. P. Gupta, Head, Department of Electrical Engineering, IIT Roorkee and Prof. Dr. Jaydev Sherma, Group Leader (Power System Engineering), for providing all the facilities to make this Dissertation a successful one.

I am also deeply thankful to all the faculty members of Power System Engineering Group for their inspirational impetus, invaluable suggestions, constructive criticism and constant encouragement.

I am extremely thankful to Mr. Bhavesh Bhalja, Research Scholar, whose guidance has been very valuable for me during my dissertation work.

I am grateful to Kapoorji, lab assistant, Power System Simulation Lab for providing me all computer and hardware facilities to carry out my dissertation work.



**(PARIKH URMIL B.)**

## ABSTRACT

---

Accurate, fast and reliable protective scheme is an important operational requirement in modern day power transmission systems. In this thesis, a new digital distance protection scheme for series compensated transmission lines is developed. The proposed distance protection scheme is comprised of three distinct stages, namely, (a) Fault Classification, (b) Selection of Faulted Section (Whether the fault is in front or behind the series capacitor) & (c) Distance Calculation and First Zone Detection. Support Vector Machine (SVM) is used for development of algorithms for all three stages. Performance of the algorithms developed for aforesaid three stages is tested on a large test data set of more than 25,000 cases generated on a model of 400kV, 300 KM transmission line with series compensation placed in the middle of the transmission line having Metal Oxide Varistor (MOV) for the protection of compensating capacitor. The simulation is carried out using well known PSCAD/ EMTDC software package. Further, performance of the developed distance protection scheme has been compared with some of the earlier approaches reported in literature for the same purpose. The results indicate that the proposed SVM based distance protection scheme is fast, accurate and robust among all the approaches discussed in this thesis for a wide variation in system and fault conditions.

# CONTENTS

---

	<b>Page No</b>
CANDIDATE'S DECLARATION	i
ACKNOWLEDGEMENT	ii
ABSTRACT	iii
<b>CHAPTER 1: INTRODUCTION</b>	<b>1</b>
1.1 Protection of Series Capacitor against Short Circuits and Over Voltages.	1
1.2 Problems in protection.	2
1.2.1 Overreaching due to Non-Linearity of protective devices of series capacitors like MOVs.	3
1.2.2 Transient Problems.	7
1.2.3 Voltage Inversion.	7
1.2.4 Current Inversion.	9
1.2.5 MOV and Overload protection Operation.	9
1.2.6 Other Concerns.	9
1.3 Literature Review.	10
1.4 Case Studies and Simulation Data Generation.	12
1.4.1 System Model.	12
1.4.2 Simulation Parameters	13
1.4.3 Simulation Cases Generated.	13
<b>CHAPTER 2: FAULT CLASSIFICATION</b>	<b>15</b>
2.1 A New Decision Tree Based Fault Classification Scheme	15
2.1.1 Fundamental Phasor Computation.	15
2.1.2 Fault Classification Technique.	16
2.1.3 Fault Classification Algorithm.	16
2.1.4 Simulation Results.	18
2.2 SVM based Fault Classification Scheme.	19
2.2.1 Introduction to SVM for Pattern Classification	19
2.2.2 Fault Classification Algorithm.	22
2.2.3 Training and Testing Dataset Generation.	23
2.2.4 Simulation Results.	23

2.2.5	Parameter Selection of SVM.	24
2.3	Fuzzy Logic Based Fault Classification Scheme.	26
2.3.1	Introduction	26
2.3.2	Fuzzy Fault Classification Scheme.	28
2.3.3	Simulation Results.	30
2.4	Comparison of Different Fault Classification Schemes.	31
<b>CHAPTER 3: FAULT ZONE IDENTIFICATION</b>		32
3.1	Introduction to Wavelet Transforms.	32
3.2	Basic Scheme.	34
3.3	Training and Testing Dataset Generation.	35
3.4	Results and Discussion.	35
3.5	Parameter Selection of SVM.	36
3.6	Choice of Mother Wavelet.	37
3.7	Further Test Results.	38
<b>CHAPTER 4: FAULT DISTANCE CALCULATION</b>		39
4.1	Algorithm based on Combined Wavelet-SVR Technique.	39
4.1.1	Introduction to Support Vector Regression (SVR).	39
4.1.2	SVR Technique for Fault Distance Calculation.	41
4.1.3	First Zone Detection Error.	42
4.1.4	Fault Distance Calculation Error.	43
4.1.5	Selection of Appropriate SVR Technique with Associated Parameter Values.	43
4.1.6	Results	44
4.2	Algorithm based on Voltage Compensation Technique.	45
4.2.1	Linearised Equivalent Model of a Series Capacitor.	45
4.2.2	Current Peak Detection.	46
4.2.3	Calculation of Voltage across SC-MOV Combination.	47
4.2.4	Simulation Results.	48
4.3	Comparison of Combined Wavelet-SVR and Voltage Compensation Techniques.	49
<b>CHAPTER 5: CONCLUSION</b>		50
<b>REFERENCES</b>		51

'CB' and air-gap 'AG' are placed across the series capacitor for protection purpose. The damping circuit 'Ld' limits the oscillatory transient current through air gap when it fires.

With short circuits on the line, the voltage across capacitor could build up to extremely high values, especially under resonant system conditions. The MOV, in this case, will limit the voltage to some predetermined safe level, typically 2 pu, where 1 pu is the voltage across capacitor with rated current flowing through it. Economics dictate an upper limit for energy dissipation required by the MOV in un-faulted line for the worst case external fault. This means that the MOV is not capable of dissipating the energy that would be generated on some internal faults. To protect the MOV under these conditions, an energy monitor calculates the energy being dissipated by MOV and triggers the air gap to divert the current away from MOV when the energy limit of MOV is reached. The gaps also have some finite energy capability and, therefore, also require a diverter which in this case is the bypass breaker.

A key advantage of adding the MOVs is a short reinsertion time. This is important in case of the un-faulted line. With only gap protection, the un-faulted line would need to have bypass breaker closed to interrupt conduction of the gap before the capacitor could be put back into service. In the case of MOV, when the external fault is cleared and the over voltage across capacitor disappears, the MOV stops conducting and the capacitor is back in service.

## **1.2 PROBLEMS IN DISTANCE PROTECTION WITH SERIES CAPACITOR**

Series Capacitors (SCs) and their over voltage protection devices, particularly Metal Oxide Varistors and Air gaps, when installed on a transmission line, create several problems for its protective relays and fault locators. The voltage and current signals produced on the transmission lines differ in a great extent for faults occurring before and after compensating capacitor.

The fault signals captured under such conditions contain different frequency components. The dominant frequency components are [1]:

1. Non fundamental decaying frequency components due to resonance between the system inductance & series capacitor including decaying DC and sub- synchronous

frequencies having frequency components varying around half the fundamental frequency value.

2. Odd harmonics due to MOV conduction during faults.
3. High frequency components caused by resonance between line capacitance & line inductance.
4. Fundamental frequency components of the steady state fault current.

Therefore, operating conditions for protective relays become unfavorable and include such phenomena as voltage or current inversion, sub-harmonic oscillations and additional transients caused by the air gaps triggered by thermal protection of the MOVs. Overreaching of distance elements due to series compensation is probably the most critical and known consequence of SCs. The opposite may happen as well, i.e. a distance protection may fail to pick up a low current fault on the protected line. All the problems are being discussed briefly in this section.

#### **1.2.1 OVERREACHING DUE TO NON-LINEARITY OF PROTECTIVE DEVICES OF SERIES CAPACITORS:**

Normally, three single-phase banks of capacitors are used for series compensation. Each capacitor must be protected against over voltages by air gaps or Metal Oxide Varistors (MOVs) or both. Under load conditions or low-current faults, the voltage drop across the SCs is below the voltage protection level: neither the air gaps nor the MOVs conduct any current. Therefore, the SC bank is equivalent to a pure reactance equal to the reactance of the actual physical capacitor. Under high current faults, the voltage drop would be far above the protection level: the gaps and/or MOVs conduct majority of the through fault current, practically by-passing the SCs. Therefore, for large through currents the SC bank is equivalent to a small resistance [1]. Between the two extremes, there are situations when a comparable amount of current flows through the SCs and MOVs as shown in Fig. 1.2 [1]:



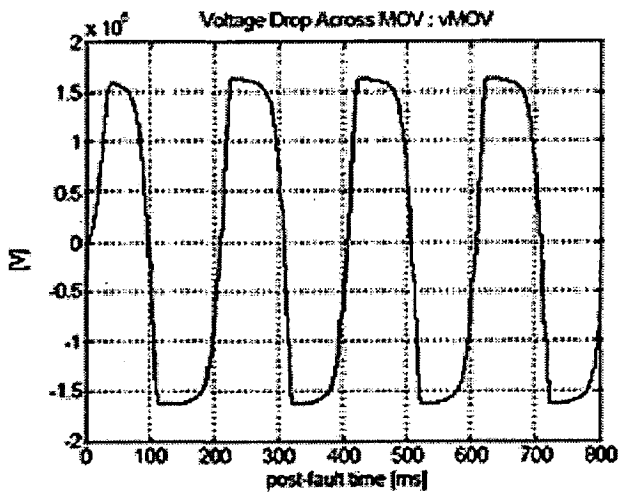


Figure 1.2(a): Voltage drop across a Conducting MOV

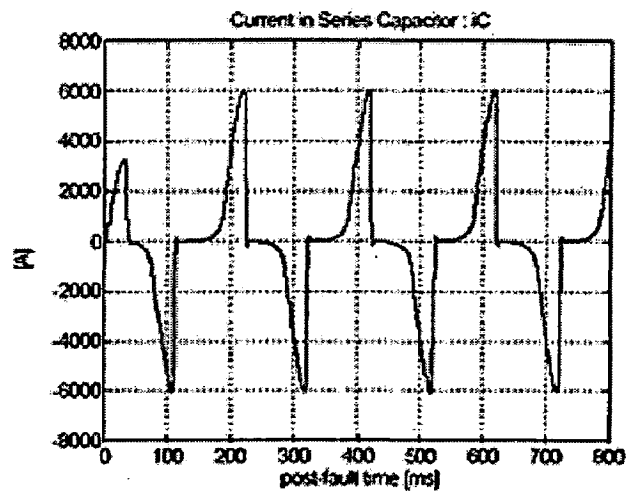


Figure 1.2(b): Current in Series Capacitor with conducting MOV

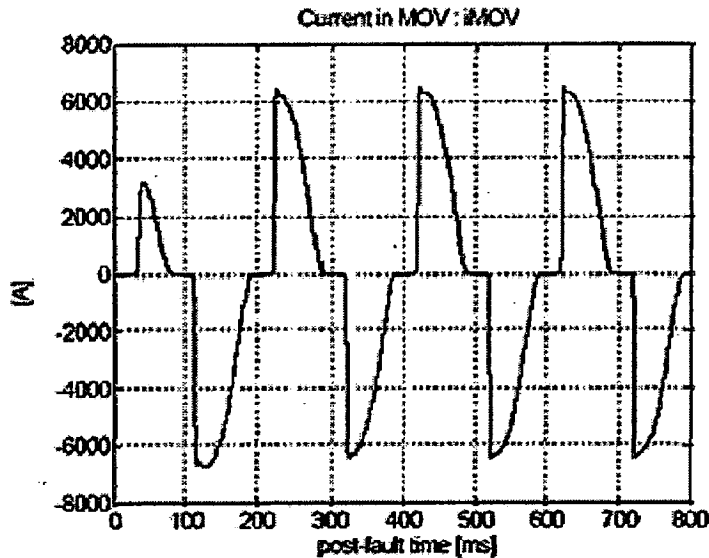


Figure 1.2 (c): Current in a conducting MOV

As the through current becomes larger, the voltage drop across the series capacitor bank assumes more rectangular shape, being limited to the voltage protection level as shown in Fig. 1.2 (a). The series capacitor conducts the current during initial half-cycles (Fig. 1.2 (b)), while the MOVs conduct during the remaining halves as shown in Fig. 1.2 (c). The through current will be the sum of both the currents. It will be shifted in leading direction with respect to the voltage drop across the bank. Relation between the fundamental frequency components of the voltage drop across the bank and the through current is resistive-capacitive impedance known as a Goldsworthy's equivalent impedance as shown in Fig. 1.3 (b) [1].

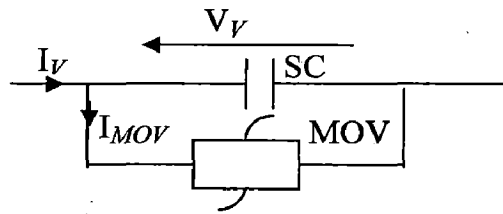


Figure 1.3(a): Circuit representation of Series Capacitor-MOV combination

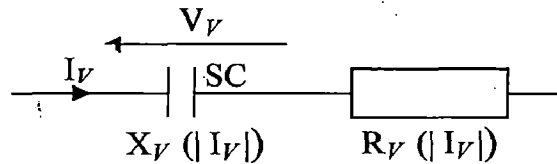


Figure 1.3(b): Equivalent fundamental frequency Impedance of Fig. 1.3(a)

In Fig. 1.3 (b),  $X_V$  and  $R_V$  represents the Goldsworthy's equivalent resistance and reactance of the combined SC-MOV arrangement. It can be realized that the equivalent SC-MOV impedance is nonlinear [2]. This is due to the fact that MOV is a non linear device whose characteristics is shown in Fig. 1.3 (c),

$$i = P \cdot \left( \frac{v}{V_{ref}} \right)^q \quad (1.1)$$

Where,  $P$  &  $V_{ref}$  are coordinates of the knee point &  $q$  is an exponent. This non-linearity of MOV introduces complexity in the impedance measurement of the conventional distance relay.

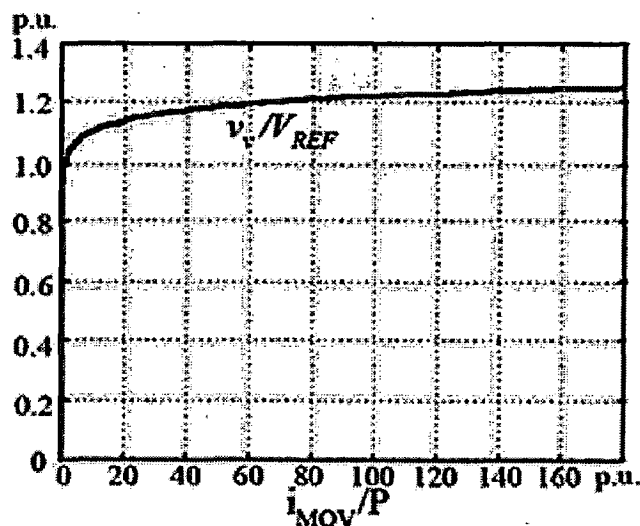


Figure 1.3 (c): Sample MOV characteristics

The concept of equivalent impedance helps to explain the basis of the problem of overreaching phenomenon. If the SCs are located between the fault and the relay potential point, the fault loop contains the line-to-fault impedance, fault resistance (if any) and the equivalent SC & MOV impedance which is nonlinear. The resistive-capacitive nature of the equivalent SC-MOV impedance shifts the apparent impedance down and to the right as shown in Fig. 1.4. As the lines are typically compensated to the tune of 50-70 %, the overreach may be as high as 50-70 % of the line impedance.

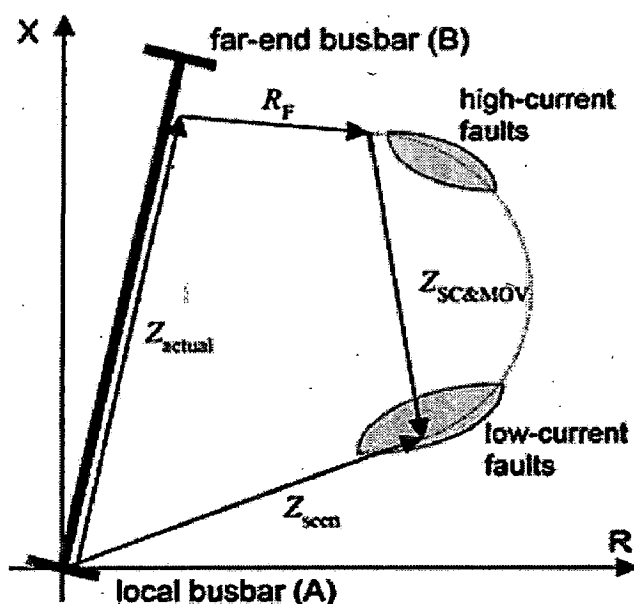


Figure 1.4: Distance element overreaching due to series compensation

During medium-current faults on the line, the apparent impedance may be shifted to the right by more than half the reactance of capacitors. This relocation may be high enough to push the apparent impedance outside the operating characteristics. In the worst case – for low-current faults – the equivalent SC & MOV impedance down by the entire reactance of the physical capacitors. This makes the failure of a distance function for a low-current close-in fault. Under such a fault, sometimes, the apparent impedance moves to the fourth quadrant of the impedance plane, resulting in problems with directional discrimination. For high-current faults, through, the equivalent SC & MOV impedance shifts the apparent impedance only slightly to the right, so, there is no danger of overreaching. Also it can be observed that, the SC & MOV bank acts as a ‘fault current stabilizer’: for larger currents the

capacitive reactance is smaller while the resistance is larger – this reduces the current as compared with a fully compensated circuit; for smaller currents, the capacitive reactance is larger – this reduces the net impedance and increases the current as compared with a non compensated circuit.

### 1.2.2 TRANSIENT PROBLEMS:

The addition of series compensation to a system will introduce several transient effects in estimating the voltage and current phasors. These effects impact protection scheme for series compensated lines as well as the protection scheme on adjacent lines. Heavy oscillations consisting of different harmonic components along with fundamental one are visible in both current and voltage signals [1].

On series compensated lines, the capacitor will introduce a sub-synchronous frequency. The frequency is dependent on the capacitor and system parameters. The natural frequency is proportional to the degree of compensation and is inversely proportional to the source impedance ratio and the fault location. Higher frequencies occur when the fault is close to the relay. The higher frequencies will not be critical for close in faults, since the capacitor MOV will typically short the capacitor for these cases. However, when a fault occurs near the end of the line, the low frequency components will cause the impedance estimate to oscillate [3]. This causes the conventional phasor computation techniques like LES or DFT to give erroneous results.

### 1.2.3 VOLTAGE INVERSION:

Voltage inversion means that the relay sees the fault on the protected line in the reverse direction [3]. This phenomenon can be explained using Fig. 1.5 as shown below. Here, a series compensated transmission line is shown, where the series capacitor is assumed to be located in the substation. In this figure,  $Z_A$  &  $Z_B$  are the impedances of the sources  $V_A$  &  $V_B$  respectively and  $Z_L$  is the total line impedance. Now, for a fault  $F_1$  occurring at a per-unit distance of 'm', the voltage profile is shown in Fig. 1.5 by a dotted line.

It can be seen that the relay 'sees' an inverted voltage at the location ' $F_1$ ' or, in other words, the relay sees this fault as a reverse fault. On the other hand, if the fault occurs at a distance further away from the substation (i.e. 'm' increases), then the relay 'sees' a positive

voltage, i.e. the relay identifies the fault to be a forward one. Thus, depending on the location of the fault, the relay either ‘sees’ a fault to be a forward one or a reverse one.

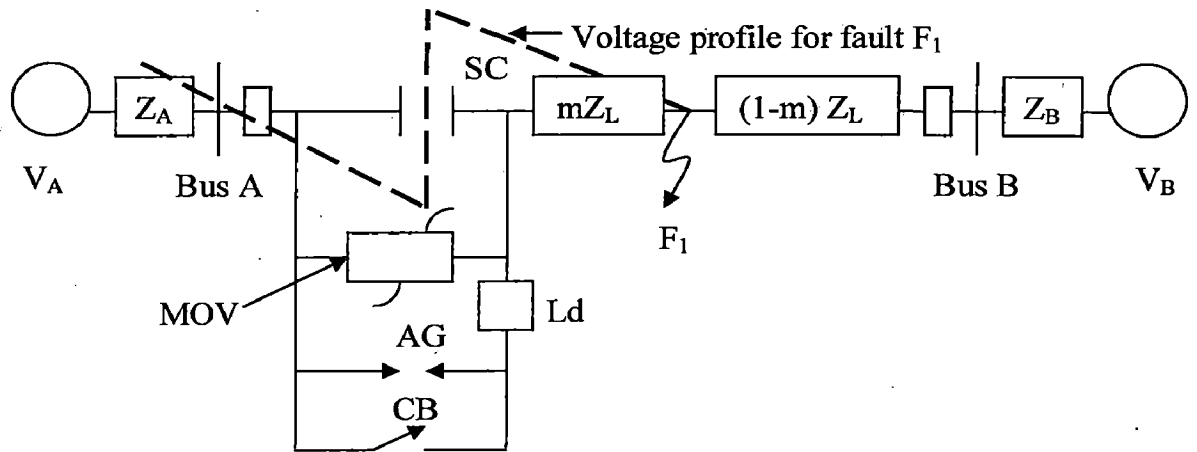


Figure 1.5: Two area power System

Now, for the bus side voltage measurement at bus A the conditions for the voltage inversion, assuming negligible resistance in the fault loop, are:

a)  $X_C > mX_L$  and

b)  $X_C < mX_L + X_A$

where,  $X_C$  is the line inductive reactance

$X_L$  is the line capacitive reactance

$m$  (p.u.) is the fault location

$X_A$  is the source A reactance.

For a fault close to the relay, voltage inversion may not occur, if the source impedance is too small (in this case, the condition (b) would not hold good). When MOV conducts for  $V_C > V_{PR}$  where  $V_C$  is the voltage across the capacitor and  $V_{PR}$  is the predetermined voltage level of the MOV, the combined reactance of MOV and SC (series capacitor) becomes less than that of  $X_C$ . As a result, the possibility of condition (a) above getting satisfied reduces. This in turn, reduces the possibility of voltage inversion. Thus, it can be said that voltage inversion may occur for faults located within certain distance on the line depending on source and line impedance, fault resistance and capacitor protective circuit.

#### 1.2.4 CURRENT INVERSION:

Current inversion means that the relay sees fault current in reverse direction due to large capacitive reactance in fault loop [3]. The voltage and current inversion can not happen simultaneously. From Fig. 1.5, for fault  $F_1$  and bus side voltage measurement, conditions for current inversion, assuming only reactance in the fault loop are:

$$\text{a) } X_C > mX_L + X_A \quad \text{and} \quad \text{b) } V_C = [X_C / \{X_C - (mX_L + X_A)\}] * V_A < V_{MAX}$$

Where,  $V_{MAX}$  is voltage that causes the gap to flash.

Current inversion may occur for the faults closer to the relay and for systems having small source impedances. The possibility of current inversion reduces under the conduction of MOV ( $V_C > V_{PR}$ ) due to the reduction of capacitive reactance to  $X_{CMOV}$ , which is less than  $X_C$ . The current inversion and voltage inversion depend upon location of series capacitor installation on the line. However, voltage and current inversion are rare phenomena.

#### 1.2.5 MOV AND OVERLOAD PROTECTION OPERATION:

Once a fault has occurred, the bypass breaker will be closed following operation of the overload protection system. This will introduce a transient in the system as the breaker arcs and the impedance seen by the relay is altered. The effect will be to increase the impedance to the fault and lower the fault current, thus altering the phasor estimation. A quick response of the MOV will reduce the capacitance and limit the impact of the sub-frequency component. The trip of the overload protection circuit will remove the capacitor from the fault loop [3].

#### 1.2.6 OTHER CONCERNS:

Asymmetrical gap flashing, high frequency components and other phenomena also influence the phasor estimates and consequently, the relay performance. Impact of high frequency components is usually reduced by filters in the relay. Asymmetric gap-flashing mainly depends upon the operation and design of the MOV overload protection and has an effect similar to an unbalanced fault. In addition, three phase bypassing is very common, thus reducing asymmetric gap flashing effect [3].

In this regard, a comprehensive analysis of the impact of the TCSC on the protection of transmission lines during system disturbances is published recently in [4]. The results

indicate that, TCSC dynamics have a significant impact on the power system protection. The transition of TCSC from a mode to another creates serious problems for the conventional relays like forward overreach, reverse overreach, mis-coordination in primary and back up protection, directional malfunction and adverse effects on distance protection schemes.

### **1.3 LITERATURE REVIEW**

The protection scheme of series compensated transmission line comprise three stages, namely, (a) fault Classification, (b) selection of faulted section (Whether the fault is in front or behind the series capacitor) & (c) distance calculation. Various techniques for the fault classification, fault zone detection and distance calculation are reported in literature.

Classification of faults means identification of the type of fault, and this information is required for fault location and accessing the extent of repair work to be carried out. Whereas, faulted Zone detection means the position of the fault with respect to series capacitor, i.e. before or after the series capacitor. Fault classification and zone detection are very challenging tasks for series compensated transmission lines. Different attempts have been made for fault classification using neural network, adaptive Kalman filtering, and fuzzy logic based approaches.

Thomas and Christopulos [5] proposed an algorithm based on traveling waves for the protection of series compensated lines. However, only a-g fault was considered in this paper. Neural network based schemes for fixed series capacitor compensated line and for TCSC compensated transmission line have been suggested in references [6, 7] and [8] respectively. Although the neural-network-based approaches have been quite successful in determining the correct fault type, the main disadvantage of ANN is that it requires a considerable amount of training effort for good performance, specially under a wide variation of operating conditions (such as system loading level, fault resistance, fault inception instance, etc.). Moreover, another disadvantage of Neural Network based algorithms is that the training may not converge in some cases, as the starting point is chosen at random and can end up in a local minimum. Furthermore, as neural networks rely on the experience gained from the training input-output examples, before practical implementation, their performances should be validated over an extensive set of test cases. The performance of the neural network based schemes suggested in [6, 7, 8] has been examined over limited test cases. Kalman filtering based technique [9] and Wavelet Transformation based technique [10, 11] have also been

suggested in the literature. Again, in all these schemes also, some limited test cases have been used for validating the performances of the developed techniques. Moreover, in [10], the sampling frequency is quite high (200 kHz), which may prove to be little inconvenient for practical implementation. An algorithm based on high frequency signals have been proposed in [12] in which specialized measurement unit consisting of stack tuner and line trap is used to capture the high frequency components of the fault signal. In this paper also, very few test cases have been used to evaluate the performance of the proposed scheme. Fuzzy logic based fault classification algorithms were proposed in [13, 14, 15]. The algorithms proposed in [13] and [14] were developed by fusion of fuzzy logic system with wavelet and Higher order statistics (HOS) respectively. However, none of these schemes was tested for wide variations in system parameters including fault inception angle, source impedances etc. Furthermore, performance of the said techniques was not tested for high resistance faults. Moreover, in [13], the sampling frequency is quite high (10 kHz), which may prove to be little inconvenient for practical implementation. Recently, Support Vector Machine (SVM) based algorithm is also developed by P.K. Dash and others [16] for fault classification and section identification purpose. However, the efficiency of this method has been demonstrated only over 200 test cases. A First Zone algorithm was proposed [17] by Saha M. et. al. The algorithm firstly estimates instantaneous values of the voltage drop across the series capacitor online, and then compensates for this signal when calculating the impedance for the faults behind series capacitors. The other impedance (without compensation) is calculated for faults in front of the series capacitors. After calculating the impedances, three special regions on the  $Z$ -plane are applied to the two impedances. A unique logic block is designed to recognize whether the fault is located in the 75-85 % of the line length i.e. first zone. However, the effectiveness of the developed technique was tested over a limited number of 2160 test cases. Also, the compensation level used was fixed at 70% in this case. In [18], an elegant voltage compensation based method has been developed for protection of series compensated transmission lines. In this method, the fault impedance is calculated as the ratio of the voltage phasor and current phasor. For fault occurring behind the series capacitor (as observed from relaying point), the voltage across the series capacitor is estimated, which is subsequently subtracted from the voltage measured by the relay to get the phasor of the voltage drop in the line. On the other hand, for the faults occurring before



the capacitor (as observed from relaying point), the voltage measured by the relay represents the voltage drop in the line and hence this voltage is used to calculate the voltage phasor. Although, this method is conceptually quite simple, it requires the knowledge of fault zone (whether before or after the capacitor).

In this thesis, a comprehensive digital distance protection scheme for series compensated transmission line using Support Vector Machine has been developed. The SVM algorithms are implemented in the MATLAB environment using Lib-SVM tool box [19, 20, 21]. The developed scheme completely integrates three aspects of digital distance protection system, i.e fault classification, fault zone identification and fault distance calculation. Upon testing on more than 25,000 fault cases with varying fault resistance, fault inception angle, pre-fault power transfer level, percentage compensation level and source impedances, the performance of the developed method has been found to be quite promising.

The simulation model of the system along with case studies is explained in the next section. In the subsequent chapters, the different algorithms and corresponding results are presented in detail.

## 1.4 CASE STUDIES AND SIMULATION DATA GENERATION

### 1.4.1 SYSTEM MODEL

The system studied in this work is illustrated in Fig. 1.6. The transmission line has been represented using the Bergeron line model in PSCAD/EMTDC [22]. The power system consists of two sources, a series capacitor (SC) along with its associated components, which is located at the midpoint of the line and associated components. To test the effectiveness of the proposed digital distance protection scheme, a large number of fault simulation studies have been carried out using the PSCAD/EMTDC [22] software.

The parameters of the study system are as follows,

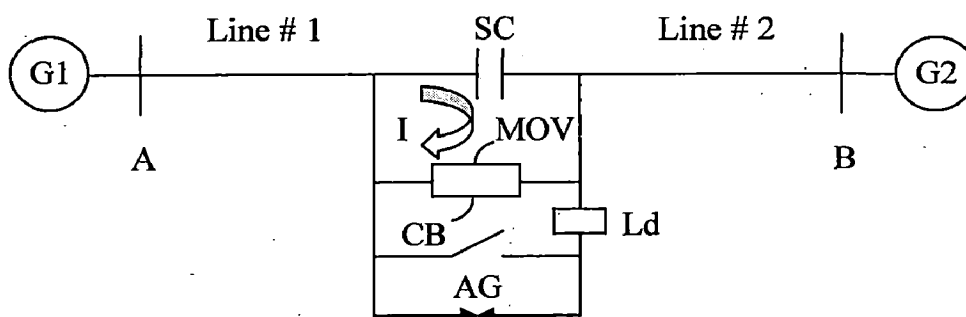


Figure 1.6: Model representation of a series compensated transmission line

#### 1.4.2 SYSTEM PARAMETERS:

##### *Source Data at both Sending and Receiving Ends:*

Positive sequence impedance =  $1.31+j15.0 \Omega$ .

Zero sequence impedance =  $2.33+j26.6 \Omega$

Voltage = 400 kV

Frequency = 50 Hz

##### *Transmission Line Data:*

Transmission-Line Data:

Length = 300 km

Voltage = 400 kV

Frequency = 50 Hz

Positive-sequence impedance =  $8.25+j94.5 \Omega$

Zero-sequence impedance =  $82.5+j308 \Omega$

Positive-sequence capacitance = 13 nF/km

Zero-sequence capacitance = 8.5 nF/km

#### 1.4.3 SIMULATION CASES GENERATED:

To test the robustness of the developed protection algorithm, the fault simulation studies have been carried out under wide variation of load angle, fault inception angle, fault resistance and fault locations. The different values of load angle, fault inception angle, fault resistance and fault positions (before and after the Series Capacitor), which have been chosen for this study, are as follows:

- (i) Load angle:  $10^\circ$ ,  $20^\circ$ ,  $30^\circ$
- (ii) Fault inception angle:  $0^\circ$ ,  $45^\circ$ ,  $80^\circ$ ,  $115^\circ$
- (iii) Fault resistance:  $0\Omega$ ,  $5\Omega$ ,  $10\Omega$ ,  $50 \Omega$ .
- (iv) Fault Locations:  $20\%$  &  $40\%$  (Before the Series Capacitor),  $60\%$  &  $80\%$  (after the Series Capacitor)

Thus,  $10 \times 3 \times 4 \times 4 \times 4 = 1920$  combinations of above mentioned parameters have been selected for a single compensation level with a fixed value of source impedance  $Z_{G1}$  and  $Z_{G2}$  at two ends of the transmission line. Moreover, a total of 15 different cases have been generated by varying the above ( $Z_{G1}$  &  $Z_{G2}$ ) two parameters. Hence,  $1920 \times 15 = 28800$  test cases have been simulated. Table 1.1 shows different values of parameters used in the generation of the 15 cases.

It is to be noted that for each and every fault simulation study, the fault duration has been assumed to be five cycles (0.1 s). The MOV conduction level has been chosen as 2.5 times the rated current and the maximum rated current has been obtained from the simulation study corresponding to  $\delta = 30^\circ$ .

TABLE 1.1: RANGE OF PARAMETER VALUES FOR TEST DATA GENERATION

Case No.	$Z_{G1}$ (%)	$Z_{G2}$ (%)	$X_c$ (%)
1-3	100	100	25,50,75
4-6	100	75	25,50,75
7-9	100	125	25,50,75
10-12	75	100	25,50,75
13-15	125	100	25,50,75

**FAULT CLASSIFICATION**

---

---

In this thesis, the fault classification task has been carried out using three different techniques listed below:

1. A New Decision Tree Based Fault Classification Scheme.
2. Support Vector Machine (SVM) based Fault Classification Scheme.
3. Fuzzy logic based fault classification Scheme.

In next sections, the three techniques have been discussed in detail. At the end, the performances of all these techniques have been compared.

**2.1 A NEW DECISION TREE BASED FAULT CLASSIFICATION SCHEME:**

In the proposed scheme, the fault classification is carried out in two steps as follows:

1. Fundamental phasor computation.
2. Fault classification.

**2.1.1 FUNDAMENTAL PHASOR COMPUTATION:**

Due to the presence of the SC and MOV/series capacitor combination at the midpoint of the line, significant differences exist between fault signals captured from line # 1 and that captured from line # 2 of Fig. 1.6, as the fault in line section 1 does not involve the loop current  $I$  during conduction stage of MOV. The fault signals captured under transient conditions contain different frequency components. The dominant frequency components are a) non fundamental decaying frequency components caused by the resonance between the system inductance & series capacitor, b) odd harmonics due to MOV conduction during faults, c) high frequency components caused by resonance between line capacitance & line inductance, d) fundamental frequency components of the steady state fault current [9]. Therefore, the fault signals are more complex to analyze in series compensated line compared to the uncompensated one. Hence, conventional filtering techniques fail to process the signals accurately in case of series compensated lines.

The technique used for phasor computation here is comprised of modified version of conventional full cycle DFT technique [23]. The technique reduces the effect of decaying

DC in the phasor computation more efficiently. In this technique, the post fault samples of a cycle time ( $N$ ) plus two samples of the next cycle i.e  $N+2$  is used for fundamental phasor computation. This algorithm is more accurate compared to conventional algorithms already in practice such as HCDFT, FCDFT or LES etc. [23].

### 2.1.2 FAULT CLASSIFICATION

The proposed technique in this thesis is single ended and uses impedance of three phases along with the zero sequence component of the fault current for fault classification purpose. In the proposed fault classification technique, it is assumed that the directional sensing unit and fault detection unit takes care of directional discrimination and fault detection problems. The technique is comprised of a logical function based algorithm, which uses three phase voltages and currents measured by conventional CT and PTs available at the relaying end. A sampling frequency of 4 kHz for a 50 Hz system is used. In this scheme,  $N+2$  post fault samples of each measurement are taken for computing the fundamental components of three phase post fault voltages and currents. Using these phasors, magnitude of post fault impedance of each phase and zero sequence post fault current are calculated. At the end, identification of faulty phase and ground involvement in the fault is carried out.

### 2.1.3 FAULT CLASSIFICATION ALGORITHM

The overall flowchart of the fault classification algorithm is shown in Fig. 2.1.

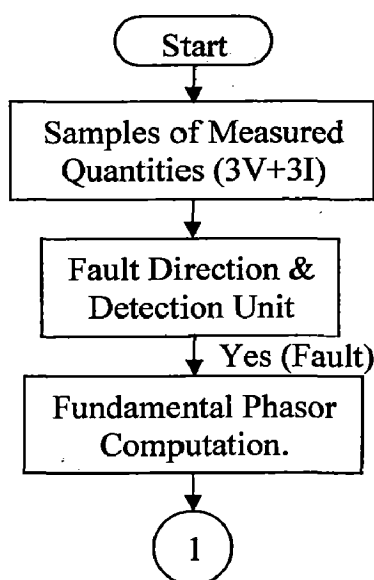


Figure 2.1: Algorithm Flowchart

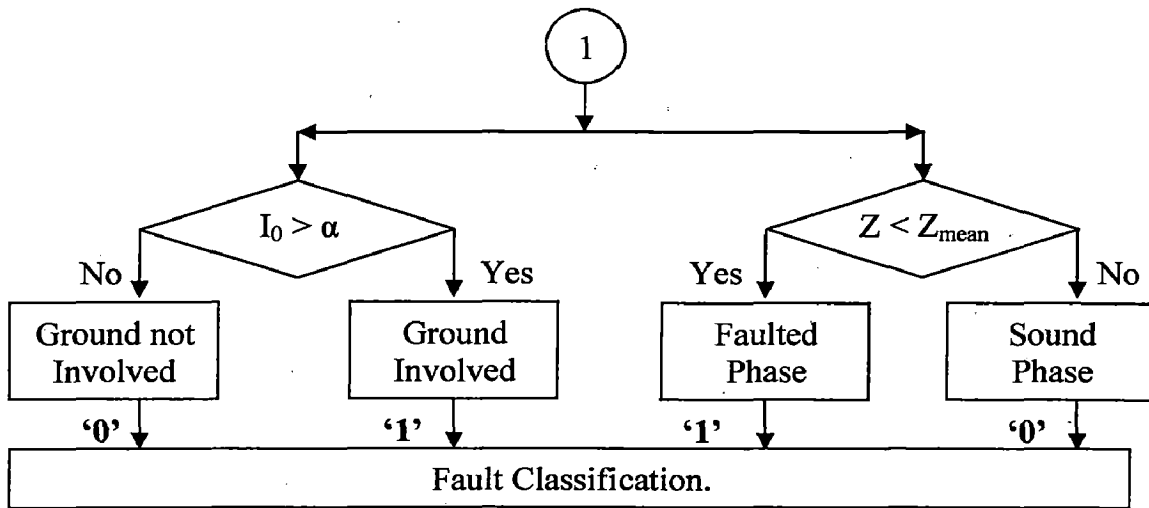


Figure 2.1: Algorithm Flowchart (Contd...)

As shown in Fig. 2.1, samples of measured quantities are taken from CT & PTs. Once the fault detection and direction estimation unit finds a fault in the forward direction, fundamental phasor computation is done using modified DFT algorithm for all the sampled values [23]. The modified DFT algorithm is given in brief in APPENDIX I. For fault classification, involvement of a phase in the fault is identified by comparing the magnitude of impedance of that phase with mean value of impedance, where,  $Z_{mean} = (Z_a + Z_b + Z_c)/3$ . If the magnitude of impedance of that phase is less than  $Z_{mean}$ , that phase is identified as a faulty phase. Fig. 2.2 shows a comparison of post fault impedance v/s mean value of impedance for a single line-to-ground fault involving phase-a. Usually it is not possible to identify involvement of ground only from fundamental components of voltages and currents. Therefore, the ground detection task is carried out using zero sequence current ( $I_0$ ). When the value of zero sequence current exceeds the threshold ( $\alpha$ ) value of 0.05, it indicates the involvement of fault with ground. Fig. 2.3 shows the simulation result. It is observed that for a fault involving ground i.e. a-g and a-b-g the value of  $I_0$  is greater than threshold, whereas for a fault not involving ground it is less than the threshold value. The fault classification block consists of four inputs representing  $a$ ,  $b$ ,  $c$  phases and ground 'g'. These inputs are assigned values '1' or '0' corresponding to the case, whether the fault is involved with that phase/ground or not.

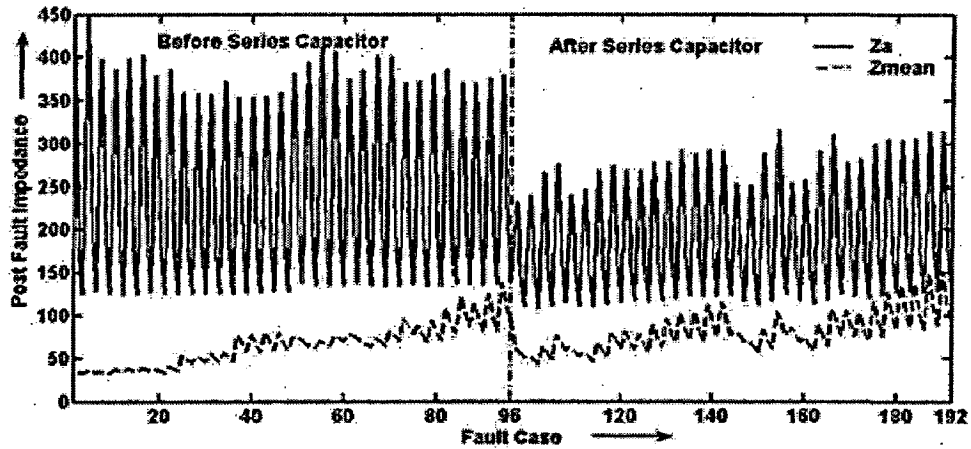


Figure 2.2:  $Z_a$  V/s  $Z_{mean}$

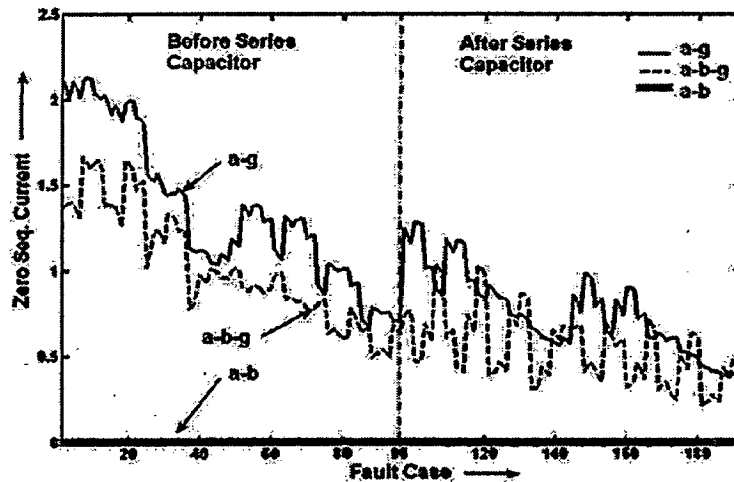


Figure 2.3:  $I_0$  for different type of faults

#### 2.1.4. SIMULATION RESULTS

Table 2.1 depicts the performance of the proposed fault classification technique for different types of faults. Here, all the simulated cases discussed in section 1.4.3 are tested for the accuracy of the proposed algorithm. It is observed from Table 2.1 that the proposed technique gives satisfactory results for double line and triple line faults (with and without ground). However, the performance of the proposed scheme is inferior for a single line-to-ground fault because the margin between mean value of impedance and individual phase impedance reduces for different extreme conditions such as high source impedance, low loading condition and low percentage compensation level. Furthermore, uneven MOV conduction in different phases can be one of the reasons for achieving lower value of percentage accuracy in the above-mentioned case.

TABLE 2.1: PERFORMANCE OF PROPOSED SCHEME FOR DIFFERENT TYPES OF FAULTS

Fault Type	No of Test Cases	Fault Classification Errors	True Fault Classification	Accuracy
L-g	8640	1601	7039	81.469%
L-L-g	8640	194	8446	97.754%
L-L-L/L-L-L-g	2880	246	2634	91.458 %
L-L	8640	723	7917	91.631 %
Total	28800	2764	26036	90.402%

The performance of the proposed technique with varying compensation level between 25% to 75% is analyzed. The results are shown in Table 2.2. It is observed from Table 2.2 that the proposed algorithm is quite accurate for a compensation level of 50%. Moreover, the proposed technique provides reasonable accuracies in case of 25% and 75% compensation levels.

TABLE 2.2: PERFORMANCE OF PROPOSED SCHEME FOR DIFFERENT COMPENSATION LEVELS

Case No	Xc %	No of Test Cases	Fault Location Errors	True Fault Location	Accuracy
1	50	9600	728	8872	92.417%
2	25	9600	978	8622	89.812 %
3	75	9600	1058	8542	88.979%
Total		25200	2764	26036	90.402 %

## 2.2 SVM BASED FAULT CLASSIFICATION SCHEME:

### 2.2.1 INTRODUCTION TO SVM FOR PATTERN CLASSIFICATION

In recent years, Support Vector Machines (SVM) have emerged as a very powerful tool to solve the classification and regression problems. For classification problems, the SVMs try to find out a hyper-plane to separate the data points according to their classes such that the separation between the classes is maximum. In that case, the hyper-plane is said to be the 'optimal hyper-plane [24].

#### *Pattern classification with support vector machines*

Consider a two class training set  $\{x_i, y_i\}_{i=1}^N$  consisting of N data points in which  $x_i$  is  $i$ -th real valued  $n$ -dimensional input vector and  $y_i$  (either +1 or -1) is the corresponding class of  $x_i$ . The hyper-plane, which successfully separates the points according to their classes, can be given by equation:  $\mathbf{w}^T \mathbf{x}_i + b = 0$ .



The two class data points and the separating hyper plane is shown in Fig. 2.4. In this equation,  $w$  and  $b$  denote a weight vector and a bias term respectively and the goal of SVM is to find out the value of  $w$  and  $b$  such that the separation between the classes is maximum. It can be shown that the separation margin ( $m$ ) is given by [24]:

$$m = \frac{2}{\|w\|}$$

Therefore, for maximizing 'm' (and thereby increasing the generalization capability of SVM),  $\|w\|$  need to be reduced. Hence, for linearly separable data, the SVM can be constructed by maximizing  $v(w)$  where,

$$v(w) = \frac{1}{2} w^T w \quad (2.1)$$

$$\text{Subject to, } y_i(w^T x_i + b) \geq 1 \quad (2.2)$$

In real life scenario, however, all practical classification problems need not be linearly separable. To cater to this scenario, a non-linear version of SVM has been developed in the literature by transforming the training data into a higher dimension space using non-linear transform is given by,

$$\Phi(x) = \{\Phi_1(x) \dots \Phi_m(x)\}^T \quad \text{Where, } m > x. \quad (2.3)$$

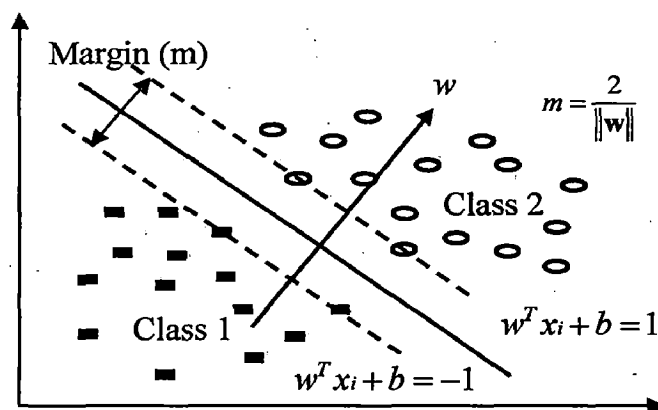


Figure 2.4: Optimal Separating Hyper plane using SVM

With this non-linear transformation, the original non-separable data may become separable in the expanded space. Hence, in this higher dimensional space, the maximum margin classifier (SVM) can be found by minimizing,

$$v(\mathbf{w}) = \frac{1}{2} \mathbf{w}^T \mathbf{w} \quad (2.4)$$

$$\text{Subject to, } y_i \{ \mathbf{w}^T \Phi(\mathbf{x}_i) + b \} \geq 1 \quad (2.5)$$

There is still no guarantee that even in the expanded space, the training data set would be linearly separable. Depending upon the choice of the function  $\Phi(\mathbf{x})$ , it may turn out that the transformed training data set is not completely linearly separable. In such cases, it would be impossible to satisfy all the constraints given by Eqn. 2.5. Hence, instead of the cost function  $v(\mathbf{w})$ , another cost function  $v(\mathbf{w}, \boldsymbol{\varepsilon})$  is used, where,

$$v(\mathbf{w}, \boldsymbol{\varepsilon}) = \frac{1}{2} \mathbf{w}^T \mathbf{w} + C \sum_{i=1}^N \varepsilon_i \quad (2.6)$$

$$\text{Subject to, } y_i \{ \mathbf{w}^T \Phi(\mathbf{x}_i) + b \} \geq 1 - \varepsilon_i; \quad \varepsilon_i > 0 \quad (2.7)$$

In Eqn. 2.7,  $\varepsilon_i; i=1,2,\dots,N$  are  $N$  non-negative slack variables, which are used to allow for training errors. The quantity  $C$  is called regularization parameter, and is always greater than zero. If the parameter  $C$  is small the separating hyper plane tends to maximize the margin ( $m$ ), while the larger  $C$  will cause hyper plane to minimize the number of misclassified points. The vectors satisfying the constraints above with the equality sign are termed as *support vectors* and the only vectors needed to determine the decision surface or the separating hyper plane. In practice, the non-linear transformation is accomplished indirectly by using so called kernel functions, which is defined by,

$$K(\mathbf{x}_i, \mathbf{x}_j) = \Phi(\mathbf{x}_i)^T \Phi(\mathbf{x}_j) \quad (2.8)$$

The most commonly used kernel functions are:

1) *Linear*:  $K(\mathbf{x}_i, \mathbf{x}_j) = \mathbf{x}_i^T \mathbf{x}_j$ .

2) *Polynomial*:  $K(\mathbf{x}_i, \mathbf{x}_j) = (\gamma \mathbf{x}_i^T \mathbf{x}_j + r)^d, \gamma > 0$ .

3) *Radial basis function (RBF)*:  $K(\mathbf{x}_i, \mathbf{x}_j) = \exp(-g \|\mathbf{x}_i - \mathbf{x}_j\|^2), g > 0$ .

4) *Sigmoid*:  $K(\mathbf{x}_i, \mathbf{x}_j) = \tanh(\gamma \mathbf{x}_i^T \mathbf{x}_j + r)$ ;

Here,  $\gamma, r$  and  $d$  are kernel parameters.

Currently in the literature, there is no method available for deciding the value of  $C$ , for choosing the best kernel function and for setting the kernel function parameters. As a result, the most appropriate kernel function and the values of kernel function parameters as well as of the parameter  $C$  are decided by trial & error procedure.

## 2.2.2 FAULT CLASSIFICATION ALGORITHM

In the fault classification scheme proposed in this work, four SVMs have been used. Out of these four SVMs, one SVM is used for each phase to determine whether that phase involved in fault or not. The fourth SVM (henceforth termed as Ground SVM) is used to determine the involvement of ground in fault. Each of the phase SVMs receives samples of one cycle duration of the current of that particular phase, where as, the ground SVM receives the samples of one cycle duration of the zero sequence current ( $I_0$ ). At the output of each SVM, the value '1' or '0' denotes the presence or absence of the fault respectively. Table 2.3 shows the fault classification format in the proposed work, while, Fig. 2.5 shows the overall flowchart of the fault classification scheme.

TABLE 2.3: FAULT CLASSIFICATION FORMAT

Sr No	Phase a	Phase b	Phase c	Ground g	Type of Fault
1	1	0	0	1	a-g
2	0	1	0	1	b-g
3	0	0	1	1	c-g
4	1	1	0	1	a-b-g
5	1	0	1	1	a-c-g
6	0	1	1	1	b-c-g
7	1	1	1	1	a-b-c-g
8	1	1	0	0	a-b
9	1	0	1	0	a-c
10	0	1	1	0	b-c

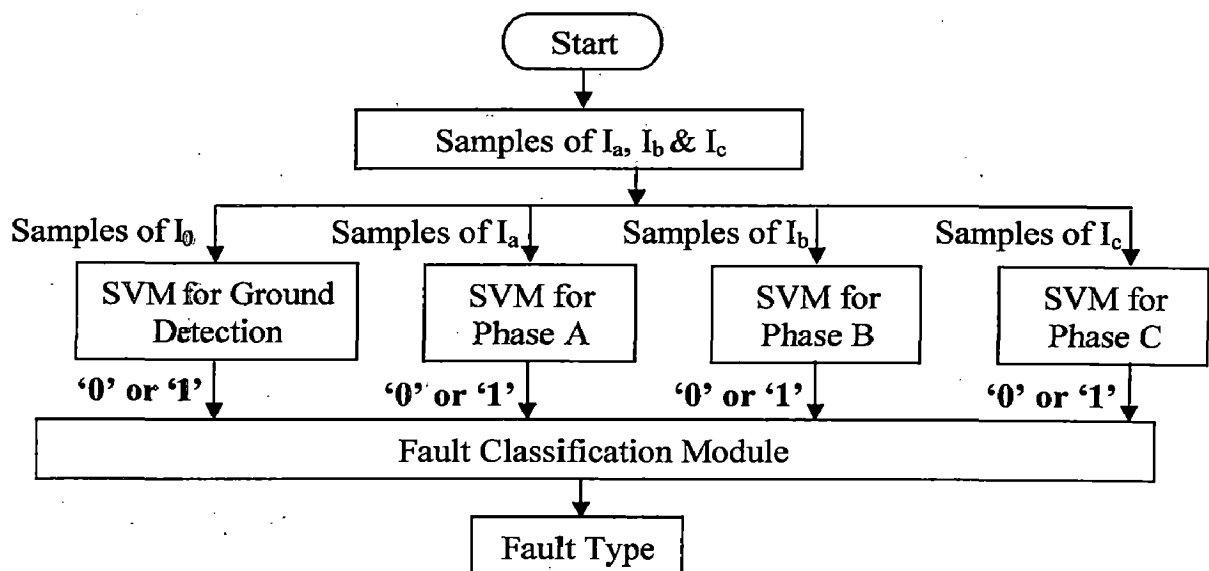


Figure 2.5: Algorithm Flowchart

### 2.2.3 TRAINING AND TESTING DATASET GENERATION

To enable all these SVMs to perform accurate fault identification, they first need to be trained. For this purpose, out of 28,800 fault cases described above, 3600 fault cases have been chosen as the training set. The details of parameters considered in the training set are given in Table 2.4. It has been observed from Table-2.4 that the training data set has been constructed by considering only the 50% compensation level of the SC. None of the 25% or 75% compensation levels has been considered in the training set.

TABLE 2.4: CASES CONSIDERED FOR TRAINING DATASET GENERATION

Case No	No of Fault cases	Parameters					
		Z <sub>G1</sub> %	Z <sub>G2</sub> %	X <sub>c</sub> %	R <sub>f</sub>	FIA	δ
1	720	100	100	50	0, 5 & 50Ω	0°, 45° & 115°	10° & 30°
2	720	100	75	50			
3	720	100	125	50			
4	720	75	100	50			
5	720	125	100	50			
Total Training data cases = 720×5 =3600							

After the SVM is trained, its performance has been tested with the remaining 25,200 fault cases. For each of this fault cases, samples of the three phase line currents along with the zero sequence current ( $I_0$ ) have been provided at input of the respective SVM. The resultant output of individual SVM denotes whether that phase/ground is involved in fault or not. Subsequently, the accuracy of the fault classification algorithm has been computed as;

$$\eta = \frac{\text{number of correct faults classified by SVM}}{25,200} \times 100$$

### 2.2.4 SIMULATION RESULTS

Upon testing over 25,200 test cases, an overall fault classification accuracy of 98.703% has been obtained by the proposed algorithm. Table 2.5 gives the performance of the proposed fault classification technique for different types of faults. It is observed from Table 2.5 that the proposed technique gives highly accurate results for all types of faults (with and without ground).

TABLE 2.5: FAULT CLASSIFICATION ACCURACY FOR DIFFERENT FAULT TYPES

Fault Type	No of Test Cases	Fault location Errors	True Fault Location	Accuracy
L-g	7560	193	7367	97.447 %
L-L-g	7560	105	7455	98.611 %
L-L-L/L-L-L-g	2520	0	2520	100.00 %
L-L	7560	29	7531	99.616%
<b>Total</b>	<b>25200</b>	<b>327</b>	<b>24873</b>	<b>98.703 %</b>

The performance of the proposed technique with varying compensation level between 25% to 75% is analyzed. The results are shown in Table 2.6. From this table, it is observed that at 50% compensation level, the accuracy of the proposed technique is highest. This is due to the fact that at this compensation level, the SVM has been trained. At 25% compensation level also, the performance of the developed method is almost same to that obtained with 50% compensation level. At 75% compensation level, however, the accuracy degrades a little, but it is still quite high and appreciable.

TABLE 2.6: FAULT CLASSIFICATION ACCURACY FOR DIFFERENT COMPENSATION LEVELS

Case No	Xc %	No of Test Cases	Fault Classification Errors	True Fault Classification	Accuracy
1	50	6000	13	5987	<b>99.983%</b>
2	25	9600	29	9571	<b>99.697%</b>
3	75	9600	285	9315	<b>97.031 %</b>
<b>Total</b>		<b>25200</b>	<b>327</b>	<b>24873</b>	<b>98.703%</b>

## 2.2.5 PARAMETER SELECTION OF SVM

Once the training samples are obtained, the next step is to determine the optimal parametric settings of SVM. In this process, the following variables: type of kernel function, its associated parameter, and regularization parameter C must be decided. For optimal Kernel - Parameter selection, the SVMs of three phases and ground are trained using different types of Kernels like RBF or Polynomial by varying the associated Kernel parameters. Thereafter, the individual trained SVMs are tested for the accuracy with the test data set. At the end, SVM models with the highest Fault Classification accuracy will be adopted. Various parameters for the SVM like regularization parameter C, degree of polynomial (p), gamma

(g) of RBF etc. are varied as: C from 1 to  $10^8$  and Gamma (g) of RBF from  $10^{-8}$  to  $10^8$  in the steps of  $10^1$  to choose the best parameters for SVM. The degree of polynomial (p) is varied from 1 to 9 in steps of 1. However, it was observed that, RBF type kernel gives the highest fault classification accuracy. Table 2.7 shows the optimal parameters giving highest fault identification accuracies for individual phase and ground SVMs using RBF kernel.

TABLE 2.7: FAULT LOCATION ACCURACY FOR DIFFERENT COMPENSATION LEVELS

SVM	Regularization Parameter 'C'	Gamma Parameter 'g'	No of Test Cases	Fault Classification Errors	True Fault Classification	Highest Accuracy achieved
I <sub>a</sub>	100	0.0045	25200	53	25147	99.7897%
I <sub>b</sub>	22	0.0026	25200	70	25130	99.7222%
I <sub>c</sub>	86682	0.00001977	25200	232	24968	99.0794%
I <sub>0</sub>	1.35	0.006	25200	0	25200	100%

Table 2.8 shows the break up of the results obtained for source impedance variations at two ends of the transmission line along with the variation in compensation level. From this table, it is observed that the developed technique is quite effective for parameter variations except for one case, where fault classification efficiency goes below 90%.

TABLE 2.8: PERFORMANCE OF PROPOSED ALGORITHM WITH DIFFERENT PARAMETERS

Case No	Xc %	Z <sub>G1</sub> %	Z <sub>G2</sub> %	No of Test Cases	Fault Classification Errors	True Fault Classification	Accuracy
1	50	100	100	1200	12	1188	99.000 %
2		75	100	1200	0	1200	100.00 %
3		125	100	1200	1	1199	99.917 %
4		100	75	1200	0	1200	100.00 %
5		100	125	1200	0	1200	100.00 %
6	25	100	100	1920	3	1917	99.843 %
7		75	100	1920	2	1918	99.895 %
8		125	100	1920	19	1901	99.010%
9		100	75	1920	3	1917	99.843 %
10		100	125	1920	2	1918	99.895 %
11	75	100	100	1920	206	1714	89.271%
12		75	100	1920	28	1892	98.541%
13		125	100	1920	10	1910	99.479 %
14		100	75	1920	29	1891	98.489%
15		100	125	1920	12	1908	99.375%
<b>Total</b>				<b>25200</b>	<b>327</b>	<b>24873</b>	<b>98.703%</b>

## 2.3 FUZZY LOGIC BASED FAULT CLASSIFICATION SCHEME:

In [15], a fuzzy logic based fault classification scheme for uncompensated transmission lines has been proposed. In this thesis, feasibility of the algorithm has also been tested for fault classification in case of series compensated transmission lines.

### 2.3.1 INTRODUCTION

The algorithm is based on the angular differences among the sequence components of the fundamental during fault current as well as their relative magnitudes. As an example, for a phase a-to-ground bolted fault in an unloaded system, the phasor diagram of sequence components of fault currents is shown in Fig. 2.6.

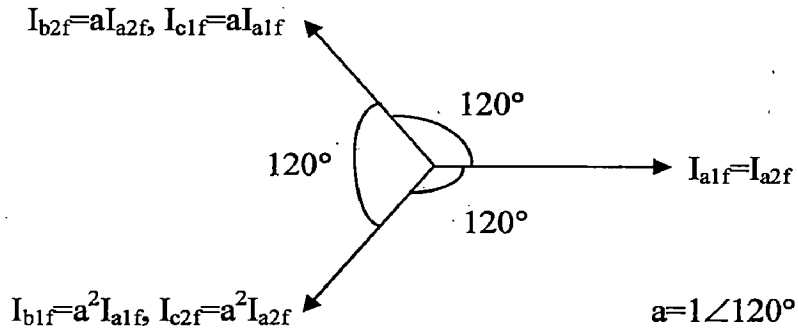


Figure 2.6: Phasor diagram of a-g fault

From Fig. 2.6, the angles between positive and negative sequence components of phase a, b and c are given by,

$$\begin{aligned} \text{Ang\_A} &= |\text{Arg}(I_{a1f}) - (I_{a2f})| = 0^\circ \\ \text{Ang\_B} &= |\text{Arg}(I_{b1f}) - (I_{b2f})| = 120^\circ \\ \text{Ang\_C} &= |\text{Arg}(I_{c1f}) - (I_{c2f})| = 120^\circ \end{aligned} \quad (2.9)$$

Also, for this type of fault, the magnitudes of  $I_{a0f}$ ,  $I_{a1f}$  and  $I_{a2f}$  are related by,

$$\text{Rof} = \left| \frac{I_{a0f}}{I_{a1f}} \right| = 1 \quad \text{and} \quad \text{R2f} = \left| \frac{I_{a2f}}{I_{a1f}} \right| = 1. \quad (2.10)$$

Similar relationships as Eqn. (2.9) and Eqn. (2.10) can also be written for other types of faults. These relationships are given in Table 2.9. In this table,

$$K = \left| \frac{Z_2}{(Z_2 + Z_0 + 3Z_f)} \right| \quad \text{and} \quad K_1 = \left| \frac{(Z_2 + 3Z_f)}{(Z_2 + Z_0 + 3Z_f)} \right| \quad (2.11)$$

In case of symmetrical fault, the zero-sequence and negative-sequence currents do not exist in the system. Hence,  $\text{ang\_A}$ ,  $\text{ang\_B}$  and  $\text{ang\_C}$  are not defined in this case. Moreover,  $R_{0f}$  &  $R_{2f}$  are also zero in this case.

TABLE 2.9: FUNDAMENTAL RELATION FOR ASYMMETRICAL FAULT S

Type of Fault	Ang_A	Ang_B	Ang_C	$R_{0f}$	$R_{2f}$
a-g	0°	120°	120°	1.0	1.0
b-g	120°	0°	120°	1.0	1.0
c-g	120°	120°	0°	1.0	1.0
a-b	60°	60°	180°	0.0	1.0
b-c	180°	60°	60°	0.0	1.0
a-c	60°	180°	60°	0.0	1.0
a-b-g	60°	60°	180°	K	$K_1$
b-c-g	180°	60°	60°	K	$K_1$
a-c-g	60°	180°	60°	K	$K_1$
symmetrical	-	-	-	0.0	0.0

It should be noted that, the relationships given in Table 2.9 are valid only for solid faults in an unloaded system. Depending upon the system parameter variations, the aforesaid five quantities of Table 2.9 will deviate from their corresponding ideal values.

To find out the ranges of variations of these five variables with the variation of the operating conditions, a large number of fault studies have been carried out under different combinations of fault location,  $R_f$ ,  $\delta$  and FIA. Also source impedances at both ends of the line as well as the compensation level have been varied. For this purpose, all the 28,800 simulated fault cases discussed in section 1.4.3 have been used. From these data, maximum, minimum and mean values of each of these five quantities given in Table 2.9 have been calculated. These quantities for all ten types of faults are given in Table 2.10.

Further, it should be noted that the technique is based on fundamental component of fault currents and hence, the fundamental phasors of three line currents are required to be evaluated. For this purpose, the same modified DFT technique as discussed in section 2.1 has been used for fundamental phasor computation.



TABLE 2.10: RANGES OF PARAMETERS FOR SIMULATED FAULT CASES

Fault Type		Ang_A	Ang_B	Ang_C	R <sub>of</sub>	R <sub>2f</sub>
Ag	Minimum	2.4985	117.4306	23.5962	0.1079	0.1533
	Mean	38.233	156.715	81.7688	0.5754	0.599
	Maximum	96.4038	179.9891	122.5694	1.319	1.1593
Bg	Minimum	23.098	2.4918	117.5082	0.1086	0.1526
	Mean	80.7572	39.2445	157.4371	0.5676	0.5927
	Maximum	122.4918	96.902	179.9066	1.321	1.1651
Cg	Minimum	118.7816	23.2649	0.1653	0.1087	0.1529
	Mean	156.1913	82.165	37.8258	0.5708	0.5972
	Maximum	179.9891	121.2184	96.7351	1.2985	1.1676
ABg	Minimum	2.0205	48.4237	117.9795	0.0547	0.1559
	Mean	43.4315	76.5699	163.3767	0.2238	0.5629
	Maximum	71.5763	122.0205	179.9811	0.4454	0.8281
ACg	Minimum	45.9114	121.9517	1.9517	0.0535	0.1537
	Mean	75.2135	164.6646	44.7865	0.22	0.5648
	Maximum	118.0483	179.9867	74.0886	0.444	0.8279
BCg	Minimum	120.5995	0.5995	42.4714	0.0563	0.1613
	Mean	164.5535	44.7265	75.2735	0.2319	0.5557
	Maximum	179.9914	77.5286	119.4005	0.4342	0.8441
ABCg	Minimum	0.0232	0.1575	0.0059	0.000484	0.0055
	Mean	78.8629	101.6196	84.699	0.0679	0.0711
	Maximum	179.6932	179.991	179.4922	0.1312	0.1463
AB	Minimum	0.2443	54.0072	112.835	0.0000000	0.2419
	Mean	38.2656	81.7493	158.244	0.0004723	0.7576
	Maximum	65.9928	127.165	179.7624	0.0095	1.0892
AC	Minimum	53.1734	112.6172	0.9624	0.0000000	0.2339
	Mean	80.6151	159.3732	39.4004	0.0005195	0.756
	Maximum	127.3828	179.865	66.8266	0.0076	1.0869
BC	Minimum	113.4585	0.5916	50.8164	0.0000000	0.2331
	Mean	158.6704	38.7046	81.3138	0.000497	0.7543
	Maximum	179.6513	69.1836	126.5415	0.009	1.0873

### 2.3.2 FUZZY FAULT CLASSIFICATION SCHEME:

From Table 2.10, approximate mean values for each of the five variables for different types of faults have been determined and are shown in Table 2.11. In this table, the different inputs (i.e. approximately 30°, approximately 90° etc.) can be represented by appropriate, corresponding fuzzy variable. With these fuzzy variables, the fuzzy rule base can be developed for identifying fault type. For all these five quantities, triangular membership functions are used, which are denoted in the form of a triplet (A, B, C) as shown in Fig. 2.7.

TABLE 2.11: APPROXIMATE MEAN VALUES OF THE DIFFERENT QUANTITIES

Type of Fault	Ang_A	Ang_B	Ang_C	Rof	R2f
a-g	30°	150°	90°	1.0	1.0
b-g	90°	30°	150°	1.0	1.0
c-g	150°	90°	30°	1.0	1.0
a-b	30°	90°	150°	0.05	1.0
b-c	150°	30°	90°	0.05	1.0
a-c	90°	150°	30°	0.05	1.0
a-b-g	30°	90°	150°	0.5	0.5
b-c-g	150°	30°	90°	0.5	0.5
a-c-g	90°	150°	30°	0.5	0.5
symmetrical	-	-	-	0.05	0.05

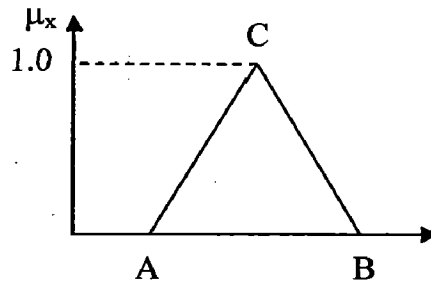


Figure 2.7: Triangular Fuzzy Membership Function

The values of the triplets of different fuzzy variables (approximately 30°, approximately 90°, low  $R_{of}$ , high  $R_{2f}$  etc.) as adopted in this thesis are given in Table 2.12.

From Table 2.11, the fuzzy rule base can be easily formed. For example, for a a-b-g fault rule will be, *If ang\_A is “approximately 30°” and ang\_B is “approximately 90°” and ang\_C is approximately 150° and Rof is “high” and R2f is “high,” then fault is “a-b-g.”* Similar rules can easily be formed for other types of faults from Table 2.11.

TABLE 2.12: FUZZY VARIABLES IN THE ANTECEDENT PARTS

Fuzzy Variable	Triplets		
	A	B	C
Approximately 30°	0°	30°	60°
Approximately 90°	60°	90°	120°
Approximately 150°	120°	150°	180°
Low- $R_{of}$	0.0	0.0	0.01
High- $R_{of}$	0.05	0.6875	1.325
Low- $R_{2f}$	0.0	0.0	0.15
High- $R_{2f}$	0.15	0.66	1.17

### 2.3.3 SIMULATION RESULTS

Table 2.13 shows the results obtained for different types of faults with compensating series capacitor placed at middle of the transmission line. It can be observed that the overall percentage error is 3.299%. Moreover, the accuracy for single line-to-ground faults is slightly inferior compared to other types of faults.

TABLE 2.13: PERFORMANCE OF FUZZY LOGIC SCHEME FOR FAULT CLASSIFICATION

Fault Type	No of Test Cases	Fault Classification Errors	True Fault Classification	Accuracy
L-g	8640	746	7894	91.365%%
L-L-g	8640	168	8472	98.055%
L-L-L/L-L-L-g	2880	0	2880	100.00 %
L-L	8640	36	8604	99.533 %
Total	28800	950	27850	96.701%

Table 2.14 shows the breakup of the fault classification results for different compensation levels. It can be observed that the technique is highly accurate for 50% and 25% compensation levels. Moreover, the proposed technique also provides appreciable results in case of 75% compensation level.

TABLE 2.14: PERFORMANCE OF FUZZY LOGIC SCHEME FOR DIFFERENT COMPENSATION LEVELS

Case No	Xc %	No of Test Cases	Fault Location Errors	True Fault Location	Accuracy
1	50	9600	120	9480	98.750%
2	25	9600	222	9378	97.687 %
3	75	9600	608	8992	93.667%
Total		25200	950	27850	96.701 %

## 2.4 COMPARISON OF DIFFERENT FAULT CLASSIFICATION SCHEMES

Table 2.15 and 2.16 gives the comparison of different fault classification techniques discussed in previous sections for different types of faults and different compensation levels respectively.

TABLE 2.15: COMPARISON OF FAULT CLASSIFICATION SCHEMES FOR DIFFERENT TYPES OF FAULTS

Type of Fault	Name of the Fault classification scheme		
	Decision Tree Based Classification Scheme	Support Vector Based Classification Scheme.	Fuzzy logic based classification Scheme.
L-g	81.469%	97.447 %	91.365%%
L-L-g	97.754%	98.611 %	98.055%
L-L-L/L-L-L-g	91.458 %	100.00 %	100.00 %
L-L	91.631 %	99.616%	99.533 %
Overall Accuracy	90.402%	98.703 %	96.701%

TABLE 2.16: COMPARISON OF FAULT CLASSIFICATION SCHEMES FOR DIFFERENT COMPENSATION LEVELS

Compensation Level	Name of the Fault classification scheme		
	Decision Tree Based Classification Scheme	Support Vector Based Classification Scheme.	Fuzzy logic based classification Scheme.
50%	92.417%	99.983%	98.750%
25%	89.812 %	99.697%	97.687 %
75%	88.979%	97.031 %	93.667%
Overall Accuracy	90.402 %	98.703 %	96.701 %

From Tables 2.15 and 2.16, it can be concluded that the support vector machine based fault classification scheme gives the highest fault classification accuracy for both different types of faults and compensation levels. Moreover, the fuzzy logic based scheme also gives good overall fault classification accuracy. However, with both decision tree and fuzzy logic based schemes, the accuracy for a compensation level of 75% and for single-line-to ground fault degrades to some extent. No such degradation of classification accuracy is observed for SVM based proposed technique. Hence, SVM based classification technique can be considered the best among these three methods.

**FAULT ZONE IDENTIFICATION**

---

---

In this thesis fault zone identification task have been carried out using combined Wavelet-SVM technique. Fault zone identification means determination of the fault location with respect to the series capacitor i.e. whether the fault is before or after the series capacitor. The said scheme is discussed in detail in this chapter.

**3.1 INTRODUCTION TO WAVELET TRANSFORMS**

The wavelet transform (WT) is a relatively new processing tool which performs time localization of different frequency components of a given signal. Therefore, by using WT, both time and frequency resolution of a given signal is accomplished. WT performs this task by using some unique analyzing functions, called mother wavelets. The unique property of the mother wavelets is that for high frequency components, the time intervals would be short whereas for low frequency components, the time intervals would be longer. Thus, WT is a quite useful technique for characterizing the transient signals occurring in a power system, and as a result, in recent times, many applications of WT for analyzing the power system transient signals have been reported in the literature. There are different types of mother wavelets available in the literature, such as Harr, Daubichies (db), Couflet (coif), symmlet (sym) etc. The choice of the mother wavelet plays a major role in the characterization of the signal under study. The mother wavelet, whose characteristics matches closely with the signal under consideration, would be the best choice. For studying power system fault signals, it has been reported in the literature that db wavelet is the most suitable one [10]. Therefore, in this work also, db wavelet has been used for the first stage analysis of the fault current signals.

Mathematically, the wavelet transform of a given signal with respect to a mother wavelet is defined in the continuous domain. However, for engineering application, a discretised version of the wavelet transform, called discrete wavelet transform (DWT) is used. Generally, DWT is implemented through multi-resolution analysis (MRA). A schematic diagram of the MRA is shown in Fig. 3.1 [25].

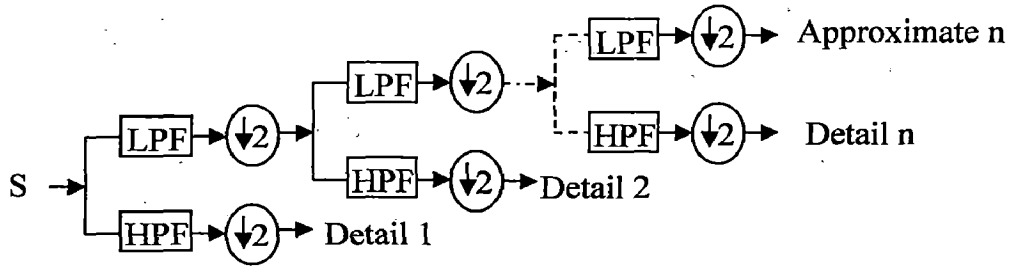


Figure 3.1: Schematic diagram of MRA

In the first stage, the original signal is decomposed into two halves of frequency components by using high pass filter (HPF) and low pass filter (LPF). In the second stage, the output of the LPF is sent again to another set of HPF and LPF to further decompose the signal into two halves of frequency components. This process is repeated till the desired level of decomposition of the original signal is achieved. If the sampling frequency of the original signal is  $f_s$ , then following sampling theorem, the highest frequency component that the signal could contain is  $f_s/2$ . Hence, in the first level, the band of frequencies between  $f_s/2$  and  $f_s/4$  would be captured. In the second level, the band of frequencies between  $f_s/4$  and  $f_s/8$  would be captured and so on. A sampling frequency of 4 KHz has been chosen in this paper and the frequency bands obtained at various levels of decomposition of WT are shown in Table 3.1.

TABLE- 3.1: FREQUENCY BANDS OF DETAIL COEFFICIENTS AT VARIOUS DECOMPOSITION LEVELS

Decomposition Level	Frequency Band obtained (Hz)
D1	1000 – 2000
D2	500 – 1000
D3	250 – 500
D4	125 – 500
D5	62.5 – 125
D6	31.25 – 62.5
D7	15.625 – 31.25
D8	7.8125 – 15.625

### 3.2 BASIC SCHEME:

The developed methodology relies on the fact that, generally, in a series compensated line, the signal contents (features) in the fault currents are different for faults occurring before and after the capacitor. Therefore, the main idea in this work is to capture the features of the fault currents (as measured at the relay location) and utilize these features in a pattern classifier to determine the fault zone (before or after the capacitor, as seen by the relay). Thus, the proposed technique consists of two stages. In the first stage, a suitable Discrete Wavelet transform (DWT) technique is employed to extract the attributes from the sampled version of the three line currents. For this purpose, samples for the duration of only one fundamental cycle have been used. In the second stage, these features are passed to a support vector machine (SVM) to decide the fault zone. The flow chart of the developed technique is shown in Fig. 3.2. In this flowchart, for the fault cases with fault occurring before the capacitor, SVM gives the output of '-1', whereas for the cases involving Series Capacitor (SC) in the fault loop, the output of the SVM will be '+1'.

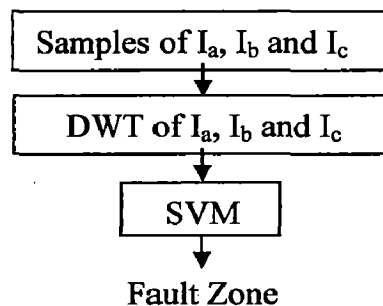


Figure 3.2: Basic Scheme

The high frequency signals above 1 kHz contained in the fault current have been considered as features of the line current in this work. These high frequency signals (attributes) have been extracted by first level decomposition of the fault current by DWT using db2 as mother wavelet. The detailed coefficients obtained by DWT are used as feature vectors or input pattern of SVM. Fig. 3.3 shows the pattern of feature vectors for training and a testing vector.

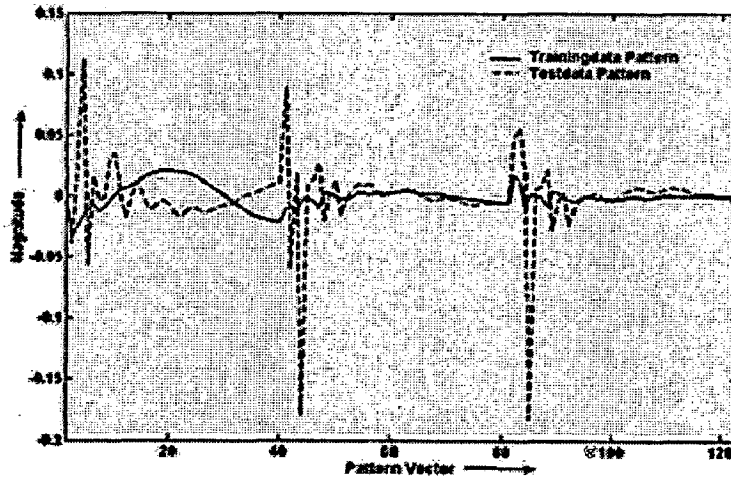


Figure 3.3: Training and Testing Patterns

After first level decomposition of the fault current of each phase, 41 co-efficients are obtained. Therefore, by decomposition of three-phase line currents, a total of 123 co-efficients are obtained. Thus, the input-output dimension of each training and testing data set is  $(123 \times 1)$ . The Gaussian RBF kernel has been used for training and testing of the SVM and the values of the parameters gamma ( $\gamma$ ) and regularization parameter ( $C$ ) have been chosen as 0.03 and  $1.08 \times 10^6$  respectively.

### 3.3 TRAINING AND TESTING DATASET GENERATION

The training-testing dataset used for this algorithm is the same as that used for the algorithm of fault classification using SVM discussed in section 2.2.3.

### 3.4 RESULTS AND DISCUSSION

Upon testing over 25,200 test cases, an overall fault zone identification accuracy of 93.167% has been obtained by the proposed algorithm. The details of the accuracies obtained for different types of faults are shown in Table 3.2.

TABLE 3.2: FAULT ZONE IDENTIFICATION ACCURACY FOR DIFFERENT FAULT TYPES

Fault Type	No of Test Cases	Fault location Errors	True Fault Location	Accuracy
L-g	7560	285	7275	96.230 %
L-L-g	7560	223	7337	97.050 %
L-L-L/L-L-L-g	2520	143	2377	94.325 %
L-L	7560	882	6678	88.333 %
<b>Total</b>	<b>25200</b>	<b>1533</b>	<b>23667</b>	<b>93.917 %</b>



From Table 3.2 it is observed that the accuracy of the developed technique is quite satisfactory for all the different types of faults involving ground. For L-L fault, however, the performance of the proposed algorithm is little inferior. However, as the probability of occurrence of a L-L fault is generally quite less compared to the probability of occurrence of faults involving ground, this limitation may probably be considered as a minor one.

The break-up of the accuracies of the proposed technique for different compensation levels is shown in Table 3.3. From this table, it is observed that at 50% compensation level, the accuracy of the proposed technique is highest. This is due to the fact that at this compensation level, the SVM has been trained. At 75% compensation level also, the performance of the developed method is quite comparable to that obtained with 50% compensation level. At 25% compensation level, however, the accuracy degrades a little.

TABLE-3.3: FAULT LOCATION ACCURACY FOR DIFFERENT COMPENSATION LEVELS

Case No	Xc %	No of Test Cases	Fault Location Errors	True Fault Location	Accuracy
1	50	6000	238	5762	96.033 %
2	25	9600	878	8722	90.854 %
3	75	9600	417	9183	95.656 %
<b>Total</b>		<b>25200</b>	<b>1533</b>	<b>23667</b>	<b>93.917 %</b>

From Table 3.2 & 3.3 it can be surmised that the accuracy of the proposed technique can probably be further enhanced by including some L-L fault cases for 25% compensation level into the training data set. In this work, however, this possibility has not been pursued further.

### 3.5 PARAMETERS OF THE SVM

In the results shown above, as mentioned earlier, the RBF kernel has been used for the SVM. Studies have also been made to investigate the performance of the SVM for polynomial Kernel and sigmoid kernels. During this investigation, the degree of polynomial ( $\gamma$ ) has been varied from 1 to 9 in step of 1. It had been found that, with polynomial kernel, the maximum classification accuracy attained was 89.45%. Whereas, using the sigmoid kernel the maximum accuracy obtained was only 74.3452%. Hence, RBF kernel had been found to be the most suitable one for this application.

For choosing the optimum values of the parameters C & g of the RBF kernel, a large

number of studies had been carried out by varying the values of these two parameters. The range of variation of these two parameters, which had been considered, is as follows: i) C; from 1 to  $10^8$  and ii) g; from  $10^{-3}$  to  $10^3$ . The classification accuracies obtained for different combinations of C and g are shown in Table 3.4.

TABLE 3.4: COMPARISON OF LOCATION ACCURACY OBTAINED WITH DIFFERENT g AND C VALUES FOR RBF-KERNEL.

Sr No	Type of Kernel: RBF		
	C	g	Fault Location Accuracy (%)
1	$0.45 \times 10^6$	0.01	88.1251
2		0.03	88.3489
3		0.05	88.8672
4	$1 \times 10^6$	0.01	92.8790
5		0.03	92.9678
6		0.05	92.4501
7	$1.05 \times 10^6$	0.01	93.3409
8		0.03	93.7103
9		0.05	93.5600
10	$1.08 \times 10^6$	0.01	93.4571
11		0.03	93.9167
12		0.05	93.7230
13	$1.15 \times 10^6$	0.01	93.3317
14		0.03	93.8492
15		0.05	93.0126
16	$1.25 \times 10^6$	0.01	93.2045
17		0.03	93.6468
18		0.05	93.3376
19	$5.75 \times 10^6$	0.01	90.0754
20		0.03	92.1865
21		0.05	90.3850

From this table, it can be observed that, the maximum classification accuracy is obtained for  $C=1.08 \times 10^6$  and  $g=0.03$ . Therefore, as already mentioned earlier, these values had been finally chosen in the work.

### 3.6 CHOICE OF MOTHER WAVELET:

Studies have also been carried out regarding suitability of different types of db mother wavelets and the classification accuracies obtained with different db mother wavelets

are shown in Table 3.5. From this table, it is observed that among different mother wavelets, db2 gives the best accuracy and therefore it has been used for feature extraction in this work.

TABLE 3.5: COMPARISON OF LOCATION ACCURACY OBTAINED WITH DIFFERENT TYPES OF MOTHER WAVELETS

Sr. No	Type of Mother Wavelet	Classification Accuracy obtained (%)
1	db1	86.78
2	<b>db2</b>	<b>93.917</b>
3	db4	88.76

### 3.7 FURTHER TEST RESULTS:

Thus for, a two step procedure for fault zone identification in which 80 samples of the three phase line currents are used, has been described. Efforts have also been made for enhancing the speed of the speed of the fault zone identification scheme further. Basically, there are two ways by which the speed of the zone identification scheme can be increased; a) by using fewer number of current samples and b) by omitting the first stage of computation (WT). Studies have been made regarding both these possibilities and the results are described briefly below.

In the first study, instead of using 80 samples, 40 samples of the three phase line currents had been used by the WT to extract the features and subsequently, these features have been used in a SVM for deciding the fault zone. The classification accuracy obtained by this approach has been found to be only 80.4167%. As this accuracy is quite low as compared to the accuracy reported earlier (93.917%), use of 40 samples (instead of 80 samples) for feature extraction can not be recommended.

In the second case, the first level computation by WT had been totally bypassed. Instead, the three phase line current samples (total  $80 \times 3 = 240$  samples) were directly used in a SVM for fault zone identification. The accuracy obtained in this investigation was only 81.5%. As this accuracy is also quite low (as compared to the accuracy described earlier), use of a single stage procedure for fault zone identification is also not very feasible.

**FAULT DISTANCE CALCULATION**

---

---

In this thesis, Fault distance calculation task has been carried out using Combined Wavelet-Support Vector Regression (SVR) technique. Further, the technique proposed in [18] based on voltage compensation has also been used for fault zone identification and distance calculation. The results obtained by both the techniques are compared at the end.

Both the algorithms to be discussed here, initially identify whether the fault is occurred within the first zone or not. In a conventional distance protection scheme, the first zone usually covers 80% of the total line length to avoid over reach and mal operation for close in faults occurring in the next line section. The algorithm for first zone and distance calculation is discussed in detail in next section, and is followed by the performance evaluation.

**4.1 ALGORITHM BASED ON COMBINED WAVELET-SVR TECHNIQUE:**

The Support Vector Regression (SVR) can be used to find a function which approximates mapping from an input domain to the real numbers based on training data maintaining all the main features that characterize the maximal margin algorithm. This unique feature of SVM regression has been exploited for the fault distance calculation. The fact that, the output values are no longer binary means that the mismatch between the hypothesis output and its training value will no longer be discrete like the SVM multi-class classification problem [26].

**4.1.1 INTRODUCTION TO SUPPORT VECTOR REGRESSION (SVR)**

The Support Vector method can also be applied to the case of regression, maintaining all the main features that characterize the maximal margin algorithm: a non-linear function is learned by a linear learning machine in a kernel-induced feature space while the capacity of the system is controlled by a parameter that does not depend on the dimensionality of the space. As in the classification case the learning algorithm minimizes a convex function and its solution is sparse.

The problem of regression is that of finding a function which approximates mapping from an input domain to the real numbers based on a training sample. The fact that the output values are no longer binary means that the mismatch between the hypothesis output and its training value will no longer be discrete. This difference between the two values is termed as the *residual* of the output, which is an indication of the accuracy of the fit at this point. It is necessary to measure the importance of this accuracy, as small residuals may be inevitable while we wish to avoid large ones. The *loss function* determines this measure. Each choice of loss function will result in a different overall strategy for performing regression. For example least squares regression uses the sum of the squares of the residuals.

In more general terms, "Regression" means, to predict labels with continuous values (or unknown values). Classification can be thought as predictions with only binary outcomes, whereas, regression as predictions that output real (floating point) numbers.

### ***Linear Regression***

Similar to SVM two class classification problem, consider a two class training set  $\{x_i, y_i\}_{i=1}^N$  consisting of N data points in which  $x_i$  is i-th real valued n-dimensional input vector. Only difference in the problem of regression is that, here  $y_i$  can be any value between normalized bounds say for an example, between 0 and 1 for each input  $x_i$ . The hyper-plane, which successfully separates the points according to their classes, can be given by equation:  $w^T x_i + b = 0$ . Here also, all the main features that characterize the maximal margin algorithm are well maintained.

### ***Non Linear Regression***

As discussed, in real life the problem to be solved may not be linear one like our problem. So, here also the non linear regression techniques are available with different types of Kernel functions like RBF, Polynomial, Sigmoid etc. which were available for SVM classification discussed already. There are two algorithms available for non linear type SVR problem.

1.  $\epsilon$ -Support Vector Regression
2.  $\mu$ -Support Vector Regression

**i)  $\epsilon$ -Support Vector Regression**

Given a set of data points,  $\{(x_1, z_1), \dots, (x_l, z_l)\}$ , such that  $x_i \in \mathbb{R}^n$  is an input and  $z_i \in \mathbb{R}^1$  is a target output, the standard form of  $\epsilon$ -support vector regression ( $\epsilon$ -SVR) is,

$$\begin{aligned} \min_{w, b, \xi, \xi^*} & \frac{1}{2} w^T w + C \sum_{i=1}^l \xi_i + C \sum_{i=1}^l \xi_i^* \\ \text{subject to} & \quad w^T \phi(x_i) + b - z_i \leq \epsilon + \xi_i \\ & \quad z_i - w^T \phi(x_i) - b \leq \epsilon + \xi_i^*, \\ & \quad \xi_i, \xi_i^* \geq 0, i = 1, 2, \dots, l \end{aligned}$$

**ii)  $\mu$ -Support Vector Regression**

For  $\mu$ -SVR, a parameter ' $\mu$ ' is used to control the number of support vectors. However, unlike Support Vector Classification, where  $\mu$  replaces with  $C$ , here  $\mu$  replaces with the parameter  $\epsilon$  of  $\epsilon$ -SVR. Furthermore, the parameter used in  $\epsilon$ -SVR is not always known to a specific level of accuracy a priori. The  $\mu$ -SVR automatically computes  $\epsilon$ .

The size of  $\epsilon$  is traded off against model complexity and slack variables  $\xi_i$  via a constant  $\mu \geq 0$ . The primal form of  $\mu$ -SVR is

$$\begin{aligned} \min_{w, b, \xi, \xi^*} & \frac{1}{2} w^T w + C(\mu \cdot \epsilon + \frac{1}{l} \sum_{i=1}^l (\xi_i + \xi_i^*)) \\ \text{subject to} & \quad w^T \phi(x_i) + b - z_i \leq \epsilon + \xi_i \\ & \quad z_i - w^T \phi(x_i) - b \leq \epsilon + \xi_i^*, \\ & \quad \xi_i, \xi_i^* \geq 0, i = 1, 2, \dots, l \end{aligned}$$

**4.1.2 SVR TECHNIQUE FOR FAULT DISTANCE CALCULATION**

The features used in fault location algorithm using combined Wavelet-SVM technique (Section 3.2) are used in this case also. The set of extracted features (123) of each fault case is used as input pattern to the SVM for the fault distance calculation. The training and testing data sets chosen for the problem are also the same as that of the case of SVM fault location technique discussed in section 3.2. The target values for training-testing data sets are the actual distances where the faults are created using simulation. These values are normalized between 0 and 1. The normalized values for various fault distances are listed in

Table 4.1. Here also, the training and testing data sets used are the same as that of the section 2.2.3.

TABLE 4.1: NORMALIZED TARGET VALUES FOR VARIOUS FAULT DISTANCES

Sr. No	Actual Fault Distance	Normalized target value
1	60 KM	0.2
2	120 KM	0.4
3	180 KM	0.6
4	240 KM	0.8
5	300 KM	1.0

After the SVM is trained, its performance has been tested with the remaining 25,200 fault cases. For each of this fault cases, attributes of the three phase line currents have been provided at the input of SVM and the resultant normalized output of the SVM has been compared with the corresponding normalized target values. The performance evaluation of the developed algorithm is done on the bases of two errors:

1. First Zone Detection Error
2. Fault Distance Calculation Error

#### 4.1.3 FIRST ZONE DETECTION ERROR

The algorithm for first zone identifies whether the fault occurred is within first zone of the line section which covers 80% of the total line length. For the simulation model used here, the total line length is 300 KM. Hence, the first zone covers 240 KM of the line length as shown in Fig. 4.1.

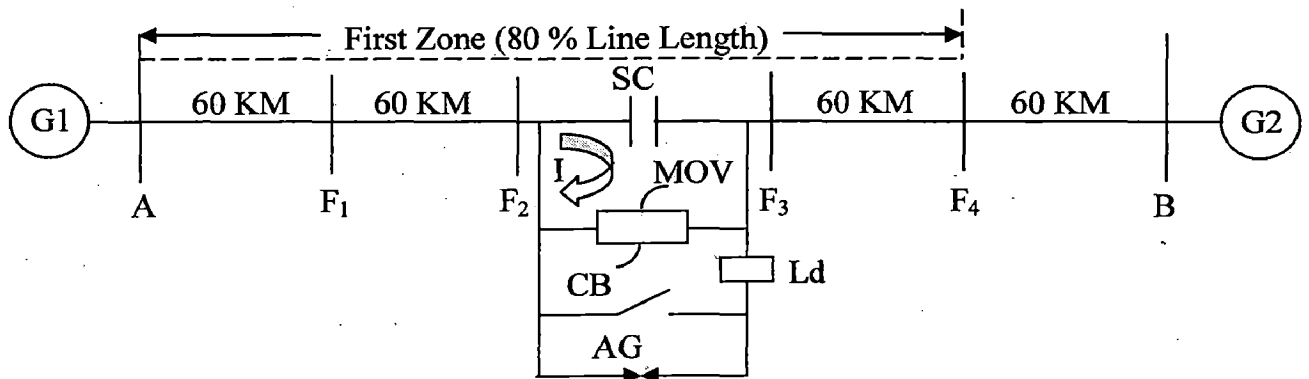


Figure 4.1: First Zone of the Simulated Series Compensated Transmission Line

The algorithm determines the position of the fault and if the fault position is within 240 KM of the line length, the trip signal is sent from the relay to isolate the line from end A. As discussed in section 1.4, the faults are created at 20%, 40%, 60% and 80% of the line length. So, for all simulated fault cases, the trip signal should be generated. Hence, the cases which do not generate trip signal are treated as the erroneous cases.

#### 4.1.4 FAULT DISTANCE CALCULATION ERROR

For distance calculation algorithm the distance of the fault point is predicted from the line end A. The predicted distance is compared with the actual fault distance, which is obtained using PSCAD/EMTDC [22] software package. The error in the distance calculation is defined by:

$$\% \text{ Error} = \left| \frac{\text{Actual Location} - \text{Estimated Location}}{\text{Total Line Length}} \right| \quad (4.1)$$

The errors for all of the 25200 test cases have been evaluated and the overall error for all of the test cases has been found out. The overall error is defined by,

$$\text{Overall Error} = \sqrt{\frac{\sum_{i=1}^{25200} (\text{Error}_i)^2}{25200}} \quad (4.2)$$

#### 4.1.5 SELECTION OF APPROPRIATE SVR TECHNIQUE WITH ASSOCIATED PARAMETER VALUES

There are two types of Support Vector Regression techniques available as discussed earlier:

1.  $\mu$ -Support Vector Regression
2.  $\epsilon$ -Support Vector Regression

Both of the SVR techniques are tested for the first zone detection and fault distance calculation. All the 25200 test cases have been considered for the performance evaluation. The results obtained shows that the performance of the algorithm is better when  $\epsilon$ -SVR technique is employed. The parameters  $e$  and  $p$  of the  $\epsilon$ -SVR technique have been varied to attain higher accuracy. The optimum values of  $e$  and  $p$  have been found to be equal to 0.001



and 0.05 respectively. The accuracy for fault zone (first zone) detection and fault distance calculation are calculated as defined in the previous section. The RBF kernel function has been used in this case as the accuracy achieved by this type of kernel is the highest.

#### 4.1.6 RESULTS:

Table 4.2 gives the results of the proposed fault classification technique for different types of faults. It is observed from Table 4.2 that the proposed technique gives satisfactory results for double line and triple line faults (with and without ground). However, the performance of the proposed scheme is inferior for the single line-to-ground type of faults.

TABLE 4.2: FAULT ZONE IDENTIFICATION ACCURACY FOR DIFFERENT FAULT TYPES

Fault Type	No of Test Cases	Fault location Errors	True Fault Location	Accuracy
L-g	7560	555	7005	<b>92.658 %</b>
L-L-g	7560	257	7303	<b>96.600 %</b>
L-L-L/L-L-L-g	2520	26	2494	<b>98.968 %</b>
L-L	7560	294	7266	<b>96.111 %</b>
<b>Total</b>	<b>25200</b>	<b>1132</b>	<b>24068</b>	<b>95.507 %</b>

The performance of the proposed technique with varying compensation level between 25% to 75% is analyzed. The results are shown in Table 4.3. It is observed from Table 4.3 that the performance of the proposed algorithm is slightly inferior for the compensation level of 50%. Moreover, the overall accuracy of the proposed algorithm is quite good hence can be used for first zone detection.

Also when checked for directional sensitivity, out of 1132 erroneous cases, only 43 cases (3.798%) detects the fault in reverse direction. Hence, the algorithm has high directional sensitivity. Furthermore, the overall error in fault distance calculation as defined by Eqn. 4.2 is only 10.77%, considering wide system parameter variations and variations in compensation level of series capacitor for a large test dataset of 25,200 cases.

TABLE 4.3: FAULT ZONE IDENTIFICATION ACCURACY FOR DIFFERENT COMPENSATION LEVELS

Case No	Xc %	No of Test Cases	Fault Location Errors	True Fault Location	Accuracy
1	50	6000	368	5632	<b>93.866 %</b>
2	25	9600	331	9269	<b>96.552 %</b>
3	75	9600	433	9167	<b>95.489%</b>
<b>Total</b>		<b>25200</b>	<b>1132</b>	<b>24068</b>	<b>95.507 %</b>

## 4.2 ALGORITHM BASED ON VOLTAGE COMPENSATION TECHNIQUE:

In the algorithm proposed in [18] based on voltage compensation technique, the voltage across the series capacitor and over voltage protective device is calculated in the relay and is subtracted from the voltage available from CVT placed at the relay end. Thus, the impedance measurement becomes immune to the MOV operation. The algorithm is discussed in detail in this section.

Consider a system having two sources  $G_1$  and  $G_2$  with series compensation (SC) placed at middle of the transmission line. When a short circuit occurs on the line, the voltage across the capacitor rises causing the nonlinear resistor of MOV to conduct, hence diverting the fault current from the SC. This causes a change in the impedance seen by the relay placed at the source end  $G_1$ . Using current signal and the SC/MOV combination characteristics, it may be possible to calculate the online voltage across the combination inside the relay. By subtracting the voltage drop across the capacitor/MOV combination from the relay signal, the new line side voltage of the SC is obtained inside the relay. If this modified voltage is used in the algorithm, the change in impedance as a result of over voltage protection operation does not appear on the calculated impedance. For calculating the voltage drop, the linearised equivalent model of the SC is used, which is discussed in next section.

### 4.2.1 LINEARISED EQUIVALENT MODEL OF A SERIES CAPACITOR:

The linearised model used here is Goldsworthy's model already discussed in section 1.2.1. The model replaces the SC-MOV combination by equivalent resistance-capacitance combination. The steady state characteristic of MOV is given by...

$$i = \left( \frac{v}{\beta} \right)^\alpha \quad (4.3)$$

Where  $\alpha = 40$  for all compensation levels and  $\beta = 93.5, 232.5724$  and  $493.0535$  for compensation levels of 25%, 50% and 75% respectively. The protection level voltage is 100.5 kV, 250 kV and 530 kV for compensation levels of 25%, 50% and 75% respectively. Taking  $I_{PU} = 1$ . Where,  $I_{PU}$  is defined by

$$\boxed{I_{pu} = \frac{I_{ph}}{I_{pr}}} \quad (4.4)$$

Where,  $I_{ph}$  is the peak of the phase current and  $I_{pr}$  is the peak of the protection level current. The latter determines the protective level and is specified by a multiple of typically 2 to 2.5 times rated bank current  $I_r$ . Equivalent resistance  $R_c'$  and equivalent capacitive reactance  $X_c'$  of the SC-MOV combination are given by Eqn. (4.5) and Eqn. (4.6) respectively as shown below [18].

$$\boxed{R_c' = X_{co}(0.0745 + 0.49 \cdot e^{-0.243I_{pu}} - 35 \cdot e^{-5.0I_{pu}} - 0.6 \cdot e^{-1.4I_{pu}})} \quad (4.5)$$

$$\boxed{X_c' = X_{co}(0.101 - 0.005749I_{pu} + 2.088 \cdot e^{-0.8566I_{pu}})} \quad (4.6)$$

The peak capacitor voltage is given by Eqn. (4.7) as shown below,

$$\boxed{V_{pk} = \sqrt{2}(I_{pr}X_{co})} \quad (4.7)$$

The only data required determining the equivalent impedance for a given current using Eqn. (4.5) and Eqn. (4.6) is  $X_{co}$  and  $I_{pr}$ . The equations apply only when the peak of the capacitor current exceeds the protective level current since below this level, the MOV is essentially out of circuit, i.e. very small conduction. To calculate the voltage across the capacitor the relay must use Eqn. (4.5) and Eqn (4.6) when MOV is conducting i.e. when  $I_{pu} > 1$ . So, it is required to calculate the peak of the phase current.

Essentially, the voltage across the capacitor can be defined in two periods: when MOV is conducting and when all fault current is passing through the capacitor. These periods depends upon the time when the current passes the value ' $I_{PU}$ '. By determining this time, the voltage across SC-MOV combination can be determined accurately. Therefore, it is required to determine whether the MOV is conducting or not. This can be carried out by calculating the peak of the phase current.

#### 4.2.2 CURRENT PEAK DETECTION:

The method for current peak detection is presented here [18]. If the line current is assumed to be sinusoidal, it can be given by,

$$i(t_1) = I_{ph} \sin(\omega t_1) \quad (4.8)$$

Where,  $\omega$  = supply frequency and  $i(t_1)$  = current at time  $t_1$ .

Similarly, current at  $t_2$  is given by,

$$i(t_2) = I_{ph} \sin(\omega t_2) \quad (4.9)$$

Where,  $t_2 = t_1 + T$  and  $T =$  sampling period.

$$\begin{aligned} i(t_1 + T) &= I_{ph} \sin[\omega(t_1 + T)] \\ \Rightarrow i(t_1 + T) &= I_{ph} \sin(\omega t_1) \cos(\omega T) + I_{ph} \cos(\omega t_1) \sin(\omega T) \end{aligned}$$

Note that, the  $\cos\omega T$  and  $\sin\omega T$  are constants since  $\omega$  and  $T$  are known. Also,  $i(t_1)$  and  $i(t_1+T)$  are available. Using Eqn. (4.8) and (4.9),

$$\begin{aligned} i(t_1 + T) &= i(t_1) \cos(\omega T) + I_{ph} \cos(\omega t_1) \sin(\omega T) \\ \Rightarrow I_{ph} \cos(\omega t_1) &= \frac{i(t_1 + T) - i(t_1) \cos(\omega T)}{\sin(\omega T)} = x \end{aligned}$$

Hence,

$$I_{ph} = \sqrt{x^2 + i^2(t_1)} \quad (4.10)$$

So, if  $i(t_1)$  and  $i(t_1+T)$  are known, the peak current  $I_{ph}$  can be obtained using eqn. (4.10).

#### 4.2.3 CALCULATION OF VOLTAGE ACROSS SC-MOV COMBINATION:

The relay calculates the phase current peak and hence,  $I_{PU}$  can be obtained inside the relay using Eqn (4.4). The voltage drop across MOV-SC combination for the aforesaid periods is calculated by the following two equations.

(a) If  $I_{PU} < 1$  or MOV not conducting:

Here, the MOV is totally bypassed and voltage drop across MOV-SC combination is the voltage across the SC.

$$V_c(t) = V_c(t-T) + \frac{1}{C} \int_{t-T}^t i(\tau) d\tau \quad (4.11)$$

Where,  $i$  is the line current and  $T$  is the sampling interval.

(b) If  $I_{PU} > 1$  or MOV is conducting:

The SC-MOV combination is replaced by the equivalent impedance denoted by Eqn. 4.5 and Eqn. 4.6. So, the voltage drop across the SC-MOV combination is given by

$$\begin{aligned} V_c &= Z_c I = R_c I - j X_c I \\ V_c(t) &= \text{Re}(V_c \times e^{j\omega t}) \end{aligned} \quad (4.12)$$

As previously explained, by calculating the voltage across the SC-MOV combination and modifying the relaying voltage signal the measured impedance becomes

immune to the MOV operation. The compensating technique is equally applicable for phase and ground elements of the distance relays. The flow chart of the whole protection scheme is shown in Fig. 4.2.

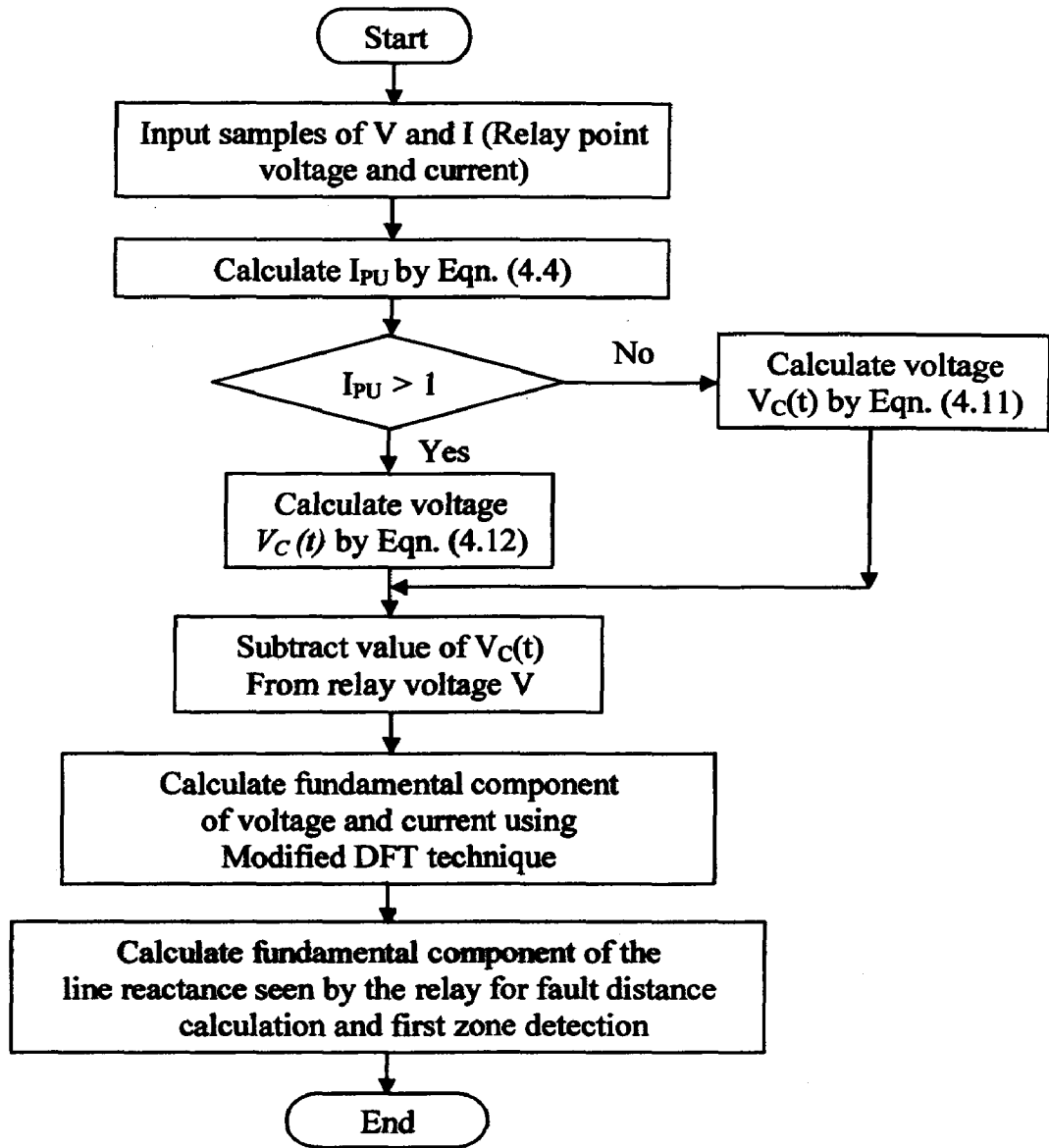


Figure 4.2: Flow chart for voltage compensation technique algorithm

#### 4.2.4 SIMULATION RESULTS

Here also, all the simulated cases (28,800) are tested for the performance of the said technique. Table 4.4 and 4.5 shows the results obtained by the technique for different types of fault and for different compensation levels respectively.

**TABLE 4.4: FAULT ZONE IDENTIFICATION ACCURACY FOR DIFFERENT FAULT TYPES**

Fault Type	No of Test Cases	Fault location Errors	True Fault Location	Accuracy
L-g	8640	2604	6036	69.861 %
L-L-g	8640	1087	7553	87.418 %
L-L-L/L-L-L-g	2880	263	2617	90.868 %
L-L	8640	1746	6894	79.791 %
<b>Total</b>	<b>28800</b>	<b>5700</b>	<b>23100</b>	<b>80.208 %</b>

**TABLE 4.5: FAULT ZONE IDENTIFICATION ACCURACY FOR DIFFERENT COMPENSATION LEVELS**

Case No	Xc %	No of Test Cases	Fault Location Errors	True Fault Location	Accuracy
1	50	9600	1671	7929	82.593 %
2	25	9600	1513	8087	84.239 %
3	75	9600	2516	7084	73.791 %
<b>Total</b>		<b>28800</b>	<b>5700</b>	<b>23100</b>	<b>80.208 %</b>

From Table 4.4, it is observed that the technique proposed in [18] fail to locate the fault accurately for wide system variations. Furthermore, the performance of the technique is even inferior for L-g type of faults, which have the highest priority of occurrence in modern power systems. The accuracy of first zone identification for 75% compensation level is also very poor as shown in Table 4.5. Furthermore, when checked for directional sensitivity, 1957 cases detect the fault in reverse direction among a total of 5700 erroneous zone detection cases (34.333%).

### **4.3 COMPARISON OF COMBINED WAVELET-SVR AND VOLTAGE COMPENSATION TECHNIQUES**

From the simulation results presented in sections 4.1.6 and 4.2.4, it is seen that, the Combined Wavelet-SVM technique developed in this thesis for fault distance calculation is more accurate and superior than the voltage compensation technique presented in [18], even for a wide variation in system parameters. Also, the Combined Wavelet-SVM based algorithm is more accurate for directional sensitivity as compared to the voltage compensation technique based algorithm.

**CONCLUSION**

---

---

The protection of series compensated transmission line differs from the uncompensated ones due to various problems encountered therein like, nonlinearity of MOVs, transient issues, voltage-current inversion and some other concerns. Moreover, the fault signals to be analyzed in this case are more complex, as they have a large percentage of DC decaying component and sub-synchronous frequency components, which are not present in large extent in the case of uncompensated lines. In this thesis, various problems associated with the protection of series compensated line have been discussed. A relaying technique, which takes into account of these problems, has been presented. The proposed method uses the samples of three line currents for one cycle duration to accomplish for this task. The technique is comprised of three stages: fault classification, fault location and fault zone identification-distance calculation. These mentioned three tasks have been carried out using SVM or fusion of Discrete Wavelet Transform with SVM.

The feasibility of the proposed algorithm has been tested on a 300 km, 400 kV series compensated transmission line for all the ten types of faults through detailed digital simulation using PSCAD/EMTDC [22]. Upon testing on more than 25,000 fault cases with varying fault resistance, fault inception angle, pre-fault power transfer level, percentage compensation level and source impedances, the performance of the developed method has been found to be quite accurate. Also, the results obtained by the developed distance protection scheme have been compared with other approaches reported in the literature. The results indicate that the proposed scheme is more reliable and exact for all the aforesaid parameter variations.



## REFERENCES

---

---

1. Bogdan Kasztenny, "Distance Protection of Series Compensated Lines Problems & Solutions", *28<sup>th</sup> Annual Western Protective Relay Conference (GE) Spokane*, pp. 1-34, Oct. 22-25, 2001,
2. R. J. Marttila, "Performance of Distance Relay Mho Elements on MOV- Protected Series – Compensated Transmission Lines", *IEEE Trans. of Power Delivery*, Vol. 7, No.34, pp. 1167-1178, Jul. 1992.
3. Damir Nvosel, Arun Phadke, M.M. Saha and S. Lindhal, "Problems and Solutions for Microprocessor Protection of Series Compensated Lines", *Sixth international Conference on Developments in Power System Protection*, Conference Publication No.-434, pp. 18-23, Mar. 25-27, 1997.
4. Mojtaba Khederzadeh and Tarlochan S. Sidhu, "Impact of TCSC on the Protection of Transmission Lines", *IEEE Trans. of Power Delivery*, Vol. 21, No.1, pp. 80-87, Jan. 2006.
5. D. W. P. Thomas and C. Christopoulos, "Ultra-High Speed Protection of Series Compensated Lines", *IEEE Trans. Power Delivery*, Vol. 7, No. 1, pp. 139-145, Jan.1992
6. Q. Y. Xuan, Y. H. Song, A. T. Johns, R. Morgan and D. Williams, "Performance of an adaptive protection scheme for series compensated EHV transmission systems using neural networks", *Electrical Power System Research*, Vol. 36, No. 1, pp. 57-66, Jan. 1996.
7. A.Y. Abdelaziz, A.M. Ibrahim, M.M. Mansour and H.E. Talaat, "Modern approaches for protection of series compensated transmission lines", *Electric Power Systems Research*, Vol. 75, pp. 85-98, May 2005.
8. Y. H. Song, A. T. Johns, Q. Y. Xuan,, "Artificial neural-network-based protective scheme for controllable series compensated EHV transmission lines:, *IEE Proc.-Gener. Transm. Distrib.*, Vol. 143, No. 6, pp. 535-540, Nov. 1996.



9. A. A. Girgis, A. A. Sallam, A. Karim El-Din, "An Adaptive Protection Scheme for Advanced Series Compensated (ASC) Transmission Lines", *IEEE Trans. Power Delivery*, Vol. 13, No. 2, pp.414-420, Apr. 1998.
10. Ashraf I. Megahed, A. Monem Moussa, A. E. Bayoumy, "Usage of Wavelet Transform in the Protection of Series-Compensated Transmission Lines", *IEEE Trans. Power Delivery*, Vol. 21, No. 3, pp. 1213-1221, Jan. 2006.
11. P. K. Dash and S. R. Samantray, "Phase selection and fault section identification in thyristor controlled series compensated line using discrete wavelet transform", *Electrical Power and Energy Systems*, Vol. 26, pp. 725-732, May 2004.
12. J.A.S.B Jayasinghe, R.K. Aggarwal, AT. Johns, Z.Q. Bo , "A Novel Non-unit Protection for Series Compensated EHV Transmission Lines Based on Fault Generated High Frequency Voltage Signals", *IEEE Trans. Power Delivery*, Vol. 13, No. 2, pp. 405-413, Jan. 1998.
13. A. K. Pradhan, A. Routray, S. Pati, and D. K. Pradhan, " Wavelet Fuzzy Combined Approach for Fault Classification of a Series-Compensated Transmission Line", *IEEE Trans. Power Delivery*, Vol. 19, no. 4, pp. 1612-1618, Oct. 2004.
14. A. K. Pradhan, A. Routray, and B. Biswal, "Higher Order Statistics - Fuzzy Integrated Scheme for Fault Classification of a Series Compensated Line", *IEEE Trans. On Power Delivery*, Vol. 19, No. 2, pp. 891-893, Apr. 2004.
15. B. Das & J.V.Reddy, "Fuzzy-logic-based fault classification scheme for digital distance protection", *IEEE Tran. Power Delivery*, Vol. 20, No.2, pp. 609-616, Apr. 2005.
16. Dash P. K.; Samantaray, S. R.; Panda, G., "Fault Classification and Section Identification of an Advanced Series-Compensated Transmission Line Using Support Vector Machine", *IEEE Trans. Power Delivery*, Vol. 22, No. 1, pp. 67-73, Jan. 2007.
17. Murari M. Saha, Bogdan Kasztenny, Eugeniusz Rosolowski and Jan Izykowski, "First Zone Algorithm for Protection of Series Compensated Lines", *IEEE Trans. On Power Delivery*, Vol. 16, No. 2, pp. 200-207, Apr. 2001.
18. F. Ghassemi, J. Goodarzi and A. T. Johns, "Method to Improve Digital Distance Relay Impedance Measurement when used in Series Compensated Lines Protected by

- a Metal Oxide Varistor”, *IEE Proc-Gener. Transm. Distrib.*, Vol. 145, No. 4, pp.403-408, Jul. 1998.
19. Chih-Chung Chang and Chih-Jen Lin, “LIBSVM-A Library for Support Vector Machines”, Available: <http://www.csie.ntu.edu.tw/~cjlin/libsvm/>
  20. “A Practical Guide to Support Vector Classification”, Chih-Wei Hsu, Chih-Chung Chang, and Chih-Jen Lin, Available: [http:// www.csie.ntu.edu.tw /~cjlin /papers /guide /guide.pdf](http://www.csie.ntu.edu.tw/~cjlin/papers/guide/guide.pdf)
  21. Hung-Te Lin, “Using (lib) SVM Tutorial”, available: [http:// ntu.csie.org /~piaip /svm /svm tutorial.html#](http://ntu.csie.org/~piaip/svm/svm_tutorial.html#)
  22. PSCAD/EMTDC Power Systems Simulation Manual, Winnipeg, MB, Canada, 1997.
  23. Sun-Liyu and Jyn-Cherng Gu, “Removal of Decaying DC in Current and Voltage Signals using a Modified Fourier Filter Algorithm”, *IEEE Trans. Power Delivery*, Vol.16, No. 3, pp. 372-379, Jul. 2001.
  24. Symon Haykin, “Neural Networks – A Comprehensive Foundation”, 2nd. ed., Prentice-Hall, 1999.
  25. Nan Zhang and M. Kezunovic, “Transmission line boundary protection using Wavelet Transform and Neural Network”, *IEEE Tran. Power Delivery*, Vol. 22, No. 2, pp. 859-869, Apr. 2007.
  26. Nello Cristianini & John, “An Introduction to Support Vector Machines and Other Kernel-based Learning Methods”, 1<sup>st</sup> ed., Cambridge University Press, 2003.